Computers in Biology and Medicine 164 (2023) 107291

Contents lists available at ScienceDirect

Computers in Biology and Medicine

journal homepage: www.elsevier.com/locate/compbiomed

Modelling cell adaptation using internal variables: Accounting for cell plasticity in continuum mathematical biology

Marina Pérez-Aliacar [a,b], Jacobo Ayensa-Jiménez [b,c], Manuel Doblaré [b,c,d,e,*]

[a] Mechanical Engineering Department, School of Engineering and Architecture, University of Zaragoza, C/ Maria de Luna, Zaragoza, 50018, Spain
[b] Engineering Research Institute of Aragón (I3A), University of Zaragoza, C/ Mariano Esquillor, Zaragoza, 50018, Spain
[c] Aragón Health Research Institute (IISAragón), Avda. San Juan Bosco, Zaragoza, 50009, Spain
[d] Centro de Investigación Biomédica en Red en Bioingeniería, Biomateriales y Nanomedicina (CIBERBBN), Avda. Monforte de Lemos, Madrid, 28029, Spain
[e] Nanjing Tech University, South Puzhu Road, Nanging, 211800, China

ARTICLE INFO

Keywords:
Cellular adaptation
Phenotypic plasticity
Glioblastoma
Hypoxia
Continuum mathematical models
Internal variables

ABSTRACT

Cellular adaptation is the ability of cells to change in response to different stimuli and environmental conditions. It occurs via phenotypic plasticity, that is, changes in gene expression derived from changes in the physiological environment. This phenomenon is important in many biological processes, in particular in cancer evolution and its treatment. Therefore, it is crucial to understand the mechanisms behind it. Specifically, the emergence of the cancer stem cell phenotype, showing enhanced proliferation and invasion rates, is an essential process in tumour progression.

We present a mathematical framework to simulate phenotypic heterogeneity in different cell populations as a result of their interaction with chemical species in their microenvironment, through a continuum model using the well-known concept of internal variables to model cell phenotype. The resulting model, derived from conservation laws, incorporates the relationship between the phenotype and the history of the stimuli to which cells have been subjected, together with the inheritance of that phenotype. To illustrate the model capabilities, it is particularised for glioblastoma adaptation to hypoxia. A parametric analysis is carried out to investigate the impact of each model parameter regulating cellular adaptation, showing that it permits reproducing different trends reported in the scientific literature. The framework can be easily adapted to any particular problem of cell plasticity, with the main limitation of having enough cells to allow working with continuum variables. With appropriate calibration and validation, it could be useful for exploring the underlying processes of cellular adaptation, as well as for proposing favourable/unfavourable conditions or treatments.

1. Introduction

Cellular adaptation comprises the changes induced in cell behaviour in response to changes in their environment. It can occur via natural selection (long term response) or via phenotypic plasticity, which is the ability of a cell with a given genotype to produce different phenotypes in reaction to environmental changes [1]. There are many examples of phenotypic plasticity in nature. For example, some butterflies develop different wing colours depending on factors such as the amount of food available [2]. Another strategy is bet-hedging, consisting in randomly diversifying into different populations so that, should the environment change, some of them would have a higher probability of survival [3]. Cells can also be reprogrammed towards stem-like phenotypes and then differentiated to other cell types [4,5]. This strategy is now used in the development of biomaterials, which are designed to induce cellular adaptation and reprogramming to improve tissue regeneration [6–8].

Epigenetics is the study of heritable changes in gene expression (phenotype) which are not caused by alterations in the DNA sequence or genotype (detailed information about epigenetic mechanisms can be found in [9,10]). Epigenetic changes can be triggered by the environment and hence, they are key in cell plasticity [10]. In a sense, epigenetics is the link between the environment and phenotypic plasticity leading to cellular adaptation [11]. Epigenetic mechanisms are responsible for cell differentiation, since all cells in our organism have the same genotype, and it is their different gene expression what characterises them [12]. Throughout our lifespan, we are subjected to epigenetic changes depending on environmental factors, such as diet, habits (e.g. smoking) and social interactions [13]. Besides, epigenetics is involved in the occurrence and progression of diverse human diseases [14,15] and, in particular, in cancer. While cancer was initially thought to be caused by the accumulation of genetic mutations, in

* Corresponding author at: Engineering Research Institute of Aragón (I3A), University of Zaragoza, C/ Mariano Esquillor, Zaragoza, 50018, Spain.
E-mail addresses: marina.perez@unizar.es (M. Pérez-Aliacar), jacoboaj@unizar.es (J. Ayensa-Jiménez), mdoblare@unizar.es (M. Doblaré).

https://doi.org/10.1016/j.compbiomed.2023.107291
Received 4 May 2023; Received in revised form 20 July 2023; Accepted 28 July 2023
Available online 1 August 2023

the past decades, epigenetics has been shown to play a central role in cancer development and progression [16,17].

Tumours are now recognised as heterogeneous cell populations, presenting both genetic and non-genetic (epigenetic) differences among them [18]. Indeed, in 2022, phenotypic plasticity was included among the cancer hallmarks, and epigenetic reprogramming as an enabling characteristic facilitating the acquisition of this hallmark capability [19]. Phenotypic plasticity explains some of the most characteristic features of cancer, such as metastasis and drug resistance, probably the main challenges for improving cancer prognosis [20]. Cells, in order to become metastatic, must acquire some plasticity following the epithelial to mesenchymal transition (EMT), by which cells increase their motility [21]. This transition is triggered by different environmental factors, such as epigenetic reprogramming or external factors like hypoxia, which are now object of important research [22]. Among the different populations present in tumours, cancer stem cells (CSCs) have gained much attention in recent years [23]. These cells are believed to drive tumour initiation and growth, as well as to be related with aggressiveness and therapy resistance [24]. In opposition to differentiated tumour cells, CSCs share capacities with normal stem cells, having a higher capacity of self-renewal. The tumour population is in permanent evolution, with cells moving from differentiated phenotypes to stem-like phenotypes and vice versa depending on the tumour microenvironment (TME) [25]. Also, the EMT has been closely related to the acquisition of stem phenotypes [26].

Hypoxia is one of the main features of solid tumours, due to their high oxygen demand and their aberrant vasculature [27]. Hypoxic tumours usually correlate with increased aggressiveness and drug resistance. Current evidence supports that hypoxia drives cells towards CSC phenotypes, whereas high oxygen levels promote differentiation [28,29]. Thus, the effects that hypoxia causes in tumours and the mechanisms behind their enhanced aggressiveness are currently a hot topic in cancer research [30]. In this work, we take the example of glioblastoma (GBM) evolution under hypoxic conditions. GBM is the most common and lethal primary brain cancer, with a 5-year survival rate of only 6.8% [31], rendering it one of the cancers with worst prognosis. Hypoxia is a defining feature of GBM, and a major concern for its prognosis, since it increases cell aggressiveness, increasing the cells capacity to proliferate and invade the surrounding tissue [32]. Hence, it is important to better understand how hypoxia triggers cellular adaptation in GBM, and in tumours in general, since it can help improving cancer prognosis and treatment response.

Mathematical models are valuable tools to understand complex phenomena relating tumours and their TME and test hypotheses regarding the effects of different environmental conditions on the adaptive response of tumours. In the last years, some mathematical models have been developed to deal with cellular phenotypic plasticity and adaptation from different perspectives, ranging from agent-based models [33–35] to continuum ones [36–39]. Here we focus on the latter type. This family constitutes the majority of adaptation models developed to date and they use well known formalisms as partial integro-differential equations which are easily implemented and allow modelling the most relevant phenomena in cancer evolution together with the interactions with the TME. Several of these models define a finite number of phenotypes that behave differently, with the transitions between them mediated by environmental conditions. This approach has been widely applied to model drug resistance [40–42], but also to other adaptation processes such as hypoxia-driven adaptation [38]. However, this discrete approach to the phenotypic state does not correspond with biological observations, in which cells go through a wide spectrum of different phenotypes caused by epigenetic changes [37]. Hence, it makes more sense to consider gene expression as a continuum variable. Very recently, some authors have followed this standpoint, defining a new *artificial* dimension corresponding to the cell's phenotypic state. Some of these models consider adaptation as driven by random effects (genetic mutations) [36], while others incorporate the effect of the environment as a key agent driving phenotypic evolution [37,39].

In this work, we propose a new mathematical framework to model cell adaptation processes and phenotypic plasticity driven by the environment. Although the equations above have been particularised here to model GBM evolution under hypoxic conditions, the framework's formulation is general and can be adapted to other biological problems of cellular adaptation after suitable definition of the different terms in the corresponding equations and identification of the involved parameters, with the only constraint that continuum hypothesis is fulfilled. The core idea of this formulation is to consider cell phenotype as a continuum variable, but instead of adding an extra dimension to the problem [37,39], the phenotype is modelled as a set of internal variables that define the cell state, and consequently the cells response. This allows an easy physical interpretation of the internal variables and their relationship with the environment, while keeping the idea of continuum phenotype. The proposed approach closely follows the concept of *state* from control systems or non-linear mechanics. Cell phenotype (or state) represents at the cell level the changes at the molecular level (e.g. epigenetic changes) that lead to alterations in the cell's gene expression and therefore in its expression. A differential equation, analogous to the ones defined for cells and chemical species, is derived to describe the evolution of each internal variable, relating its change with different signal levels coming from the TME. The activation functions regulating cell behaviour are now also dependent on those internal variables. Thus, the proposed framework allows to incorporate cell response to environmental changes as well as the reversibility and inheritance typical of phenotypic changes.

The framework is first formulated in Section 2, for an arbitrary number of cell populations, chemical species and internal variables. Then, we particularise it to the case of GBM evolution under hypoxic conditions, the example chosen to illustrate the model capabilities. In Section 3, we present the results derived from the numerical simulations perform and study the influence of the parameters and the oxygenation conditions. In Section 4, we discuss the capabilities and the results of our approach to situate it within the existing approaches to model cell adaptation in the literature. Finally, Section 5 presents the main conclusions of the work.

2. Mathematical framework

In this section, we present the general mathematical framework developed to describe cell adaptation processes and phenotypic heterogeneity in tumour evolution. This framework can then be particularised to simulate a wide range of different problems, depending on the precise conditions and parameters. In this paper, we focus on GBM evolution under hypoxic conditions.

2.1. General framework

The starting point is a previously published continuum model [43,44] describing the spatio-temporal evolution of different cell populations and chemical species constituting the TME. In what follows, T and X are used to represent the temporal and spatial coordinates, respectively. All variables are considered at the population level, within a continuum framework. Considering the concentration of m cell populations $C_i = C_i(X,T)$ $(i = 1,\dots,m)$ and n chemical species $S_i = S_i(X,T)$ $(i = 1,\dots,n)$, we can write a vector of field solutions $\boldsymbol{U}$ with $m+n$ components, formed as:

$$\boldsymbol{U} = [C_1,\dots,C_m,S_1,\dots,S_n].$$

The transport equation for each component U_i is then written as:

$$\frac{\partial U_i}{\partial T} = -\boldsymbol{\nabla}\cdot\boldsymbol{q}_i + F_i, \quad i = 1,\dots,m+n. \tag{1}$$

In Eq. (1), $\boldsymbol{q}_i$ is the flux term, which in general can include both diffusive and convective terms. Analogously, F_i is the source term. In

the case of cell populations, the source term F_i comprises proliferation and death:

$$F_i = f_i U_i - d_i U_i, \quad i = 1, \dots, m, \tag{2}$$

with f_i the growth rate and d_i the death rate.

For the chemical species, the source term includes the phenomena of decay, as well as production and/or consumption by cells. We can therefore write these terms as:

$$F_i = -d_i U_i + \sum_{j=1}^{m} U_j f_{ij}, \quad i = m+1, \dots, n, \tag{3}$$

with d_i the decay rate, and f_{ij} the function modelling the consumption or production rate of the ith species by the jth cell population. In general, all the aforementioned terms and functions ($\boldsymbol{q}_i$, f_i, d_i, f_{ij}) may depend on any solution field and their derivatives. That is, every phenomena involved in cell evolution can depend on the current cell and species concentrations and on the changes in these quantities. Their particular functional form will depend on the problem in hands, and will be defined later for our reference problem, GBM evolution.

Once this primary model has been defined, we extend it to incorporate the phenomenon of cell adaptation, taking into account the cell history and how they keep "in memory" their past states. To do that, we introduce the concept of cell state (or phenotypic state) [45], which is described by one or more internal variables, that jointly represent the current phenotypic state of the cell. This is based on the state theory, widely used in other disciplines such as control theory [46] or non-linear mechanics [47] as a way to model phenomena that are dependent on past states. These variables constitute a macroscopic representation of the microscopic changes inside a cell that lead to phenotypic heterogeneity; examples include epigenetic changes [10, 48].

In general, we consider that the state of each cell population i can be fully described by r_i internal variables, accounting for the cell phenotypic changes in response to different intrinsic or extrinsic stimuli. Each variable must lie within its corresponding state space, which comprises the set of all possible configurations. Let V_{ik} denote the kth internal variable affecting the cell population U_i, for $i = 1, \dots, m$, with $V_{ik} \in [0, V_{ik}^{\max}]$. We can write the corresponding evolution equation as:

$$\frac{\partial V_{ik}}{\partial T} = \Omega_{ik} - \Lambda_{ik} V_{ik} + (\beta_{ik} - 1) f_i V_{ik} - \frac{1}{U_i} \boldsymbol{q}_i \cdot \boldsymbol{\nabla} V_{ik}, \quad i = 1, \dots, m, \quad k = 1, \dots, r_i. \tag{4}$$

Since this is a population model, internal variables are measured in the corresponding units per unit cell, expressing the average epigenetic changes per cell in the population of a Representative Volume Element (RVE) that lead to the current phenotypic state, as usual in continuum physics. The details of the mathematical derivation of Eq. (4), from the perspective of conservation laws, can be found in Appendix A. The meaning of the different terms in Eq. (4) is detailed next:

- In the first term, Ω_{ik} represents the function of epigenetic changes acquisition and may depend on a combination of external stimuli, their derivatives, and the current level of the internal variables themselves. This allows to model cell adaptation as a response to environmental changes.
- The second term in Eq. (4) is the decay term, with Λ_{ik} the decay coefficient. This term accounts for the natural reparation paths that cells follow to overcome genetic and epigenetic mutations, which are, in general, reversible [49–51].
- The third term takes into account the fact that epigenetic changes may be inherited through cell division [52–54]. In this regard, the term is proportional to the growth rate in cells (f_i) through the coefficient β_{ik}. If $\beta_{ik} = 1$, daughter cells inherit the same phenotypic state as their progenitor, whereas if $\beta_{ik} < 1$, only a percentage of daughter cells inherits the state of the parents. Otherwise, this could be interpreted as a partial repair of the phenotypic changes present in those parent cells.
- Finally, the last term is a convection term, necessary to adapt the state equation to our Eulerian framework (see Appendix A for the details). Each internal variable V_{ik} is convected with the flux term $\boldsymbol{q}_i$ of its related cell population U_i.

Lastly, we must define the effect that internal variables may have on cell behaviour. In the most general case, the set of internal variables $\boldsymbol{V}_i = (V_{ik})$, $k = 1, \dots, r_i$, associated with the population U_i, (for $i = 1, \dots, m$, since we assume that internal variables affect cell behaviour, but not chemical species) could affect every mechanism involved in the evolution of this population, so we would have:

$$\begin{aligned}
\boldsymbol{q}_i &= \boldsymbol{q}_i\left(\boldsymbol{U}, \boldsymbol{\nabla U}, \boldsymbol{V}_i\right), && i = 1, \dots, m, \\
f_i &= f_i\left(\boldsymbol{U}, \boldsymbol{\nabla U}, \boldsymbol{V}_i\right), && i = 1, \dots, m, \\
d_i &= f_i\left(\boldsymbol{U}, \boldsymbol{\nabla U}, \boldsymbol{V}_i\right), && i = 1, \dots, m, \\
f_{ij} &= f_{ij}\left(\boldsymbol{U}, \boldsymbol{\nabla U}, \boldsymbol{V}_i\right), && i = m+1, \dots, n, \qquad j = 1, \dots, m.
\end{aligned}$$

2.2. One-dimensional model of GBM evolution under hypoxic conditions

Next, we particularise the proposed general model to a specific problem, namely the evolution of GBM subjected to oxygen variations. For the sake of simplicity in the implementation and computations, we shall consider a one-dimensional model with two cell populations, corresponding to alive (C_a) and dead (C_d) cells respectively, a chemical species which is oxygen (S) and an internal variable (V), accounting for the effects of hypoxia on the phenotypic state of GBM cells.

This model is based on a previous work [55], which is extended by incorporating this internal variable, thus allowing for the simulation of more complex processes such as those of cell memory and adaptation. The reader is therefore referred to [55] for further details about the model and the physical meaning of its parameters and functions.

The equations governing the evolution of the concentration of alive and dead cells are:

$$\frac{\partial C_\mathrm{a}}{\partial T} = \frac{\partial}{\partial X}\left(D_\mathrm{C} \frac{\partial C_\mathrm{a}}{\partial X} - M_\mathrm{C} C_\mathrm{a} \frac{\partial S}{\partial X}\right) + G_\mathrm{C} C_\mathrm{a} - N_\mathrm{C} C_\mathrm{a}, \tag{5}$$

$$\frac{\partial C_\mathrm{d}}{\partial T} = N_\mathrm{C} C_\mathrm{a}, \tag{6}$$

where D_C is the diffusion term and M_C is the chemotaxis term. They jointly model cell movement, both in a random way (diffusion or pedesis) and towards oxygen gradients (chemotaxis). With regards to the source term, it comprises cell proliferation and death through the terms G_C and N_C respectively.

The corresponding coefficients may be written as:

$$D_\mathrm{C} = K_\mathrm{p} \Psi_\mathrm{mot}(V), \tag{7a}$$

$$M_\mathrm{C} = K_\mathrm{ch} \Pi_\mathrm{ch}(S) F_\mathrm{sat}(C_\mathrm{a}) \Psi_\mathrm{mot}(V), \tag{7b}$$

$$G_\mathrm{C} = K_\mathrm{gr} \Pi_\mathrm{gr}(S) F_\mathrm{sat}(C_\mathrm{a}) \Psi_\mathrm{gr}(V), \tag{7c}$$

$$N_\mathrm{C} = K_\mathrm{d} \Pi_\mathrm{d}(S) \Psi_\mathrm{d}(V). \tag{7d}$$

As can be seen in the above equations, all terms may be affected by the phenotypic state through the Ψ functions, which will be detailed later, as we define more precisely the internal variable V, its meaning and the hypotheses related to its effects on cell behaviour.

The diffusion or pedesis term (Eq. (7a)) is considered constant (except for the influence of phenotypic changes), with K_p the pedesis coefficient.

Both chemotaxis (Eq. (7b)) and proliferation (Eq. (7c)) are regulated by the *go or grow* hypothesis [56] in GBM evolution, which states that cells spend their resources either in proliferating or migrating, depending on the oxygen level and, in particular, on the hypoxia threshold S^H. To model this dependence with oxygen, we use for both phenomena the ReLU-like activation functions Π_ch, Π_gr [55]:

$$\Pi_\mathrm{ch}(S; S^H) = \begin{cases} 1 - S/S^H & \text{if} \quad 0 \le S \le S^H \\ 0 & \text{if} \quad S > S^H \end{cases},$$

$$\Pi_{\mathrm{gr}}(S;S^H)=\begin{cases} S/S^H & \text{if} \quad 0\le S\le S^H \\ 1 & \text{if} \quad S>S^H \end{cases}.$$

Also, both phenomena are restricted by space considerations assuming that cells cannot proliferate nor migrate in saturated areas [55,57] by means of a logistic growth model. Hence, we define F_{sat} to take into account this effect:

$$F_{\mathrm{sat}}(C_{\mathrm{a}};C_{\mathrm{sat}})=1-\frac{C_{\mathrm{a}}}{C_{\mathrm{sat}}}.$$

As for the coefficients regulating these phenomena, K_{ch} is the chemotaxis coefficient, while K_{gr} is the characteristic growth rate.

Cell death (Eq. (7d)) is regulated by K_{d}, the characteristic death rate, also depending on the oxygen concentration, with cells mainly dying below an anoxia threshold. This is modelled with an hyperbolic tangent activation function, depending both on a location parameter S^A and a spread parameter ΔS^A, to allow stochastic death (apoptosis) as well [55]:

$$\Pi_{\mathrm{d}}(S;S^A,\Delta S^A)=\frac{1}{2}\left(1-\tanh\left(\frac{S-S^A}{\Delta S^A}\right)\right).$$

Moving on to chemical species, the governing equation for the oxygen concentration is:

$$\frac{\partial S}{\partial T}=\frac{\partial}{\partial X}\left(D_S\frac{\partial S}{\partial X}\right)-G_S C_{\mathrm{a}}. \tag{8}$$

As can be seen in Eq. (8), the evolution of oxygen is driven by diffusion through the diffusion term D_S and by a source term accounting for cell oxygen uptake G_S. These terms are written as:

$$D_S=K_f, \tag{9a}$$

$$G_S=K_{\mathrm{u}}\Pi_{\mathrm{u}}(S)\Psi_{\mathrm{u}}(V). \tag{9b}$$

As for the cells, the oxygen diffusion term (Eq. (9a)) is constant, with K_f the diffusion coefficient. Oxygen uptake by alive cells (Eq. (9b)) is regulated by the uptake rate K_{u} and Π_{u}, a nonlinear correction function accounting for the dependence between cell uptake and the oxygen level, following oxygen consumption kinetics [58]:

$$\Pi_{\mathrm{u}}(S;S^M)=\frac{S}{S+S^M},$$

with S^M the Michaelis–Menten constant. The value of the parameters regarding GBM evolution have been obtained from [55], where they were fitted to different *in vitro* experiments in microfluidic devices.

Finally, we define an internal variable V which models the effects of hypoxia on cell state. GBM cells are known to undergo phenotypic changes under hypoxia, which promote their dedifferentiation towards a CSC phenotype [59]. The variable V represents the state of the cell (comprising factors such as gene expression levels or the number and position of DNA methylation) in an averaged macroscopic sense in the RVE population. It is bounded, so $V\in[0,V_{\max}]$. When $V=0$, the state of the cell corresponds to a totally differentiated GBM cell, while for $V=V_{\max}$, the cell behaves like a cancer stem cell. The governing equation for the evolution of the internal variable is phenomenologically expressed as:

$$\frac{\partial V}{\partial T}=\Omega-\Lambda V+(\beta-1)f_{\mathrm{C}}V+\frac{1}{C_{\mathrm{a}}}\frac{\partial V}{\partial X}\left(D_{\mathrm{C}}\frac{\partial C_{\mathrm{a}}}{\partial X}-K_{\mathrm{C}}C_{\mathrm{a}}\frac{\partial S}{\partial X}\right). \tag{10}$$

In absence of suitable experimental data, it is difficult to accurately define the functional forms as well as the value of the parameters involved in Eq. (10). Hence, in what follows we propose reasonable functional forms and parameters which may help us to show the potential of the model for qualitatively reproducing biologically-consistent behaviours, in compliance with what has been reported in literature.

We consider that the phenotypic changes are driven by external factors, in particular by the oxygen level, such that cells go towards a more stem like phenotype when the oxygen level is below the hypoxic threshold S^H while cells may differentiate again when the oxygen level is above S^H. To model this, and taking into account that V is bounded, we define Ω as:

$$\Omega=\Theta^+\left(1-\frac{V}{V_{\max}}\right)+\Theta^-\frac{V}{V_{\max}},$$

with $\Theta^+=\max(0,\Theta)$, $\Theta^-=\min(-\Theta,0)$ and the function Θ defined as:

$$\Theta=K_V(1-\gamma F(S)),$$

where K_V is the rate at which epigenetic changes are acquired (i.e., the rate at which the phenotypic state is modified) and $\gamma\in[1,2]$ is the parameter regulating whether cells move towards a differentiated phenotype when $S>S^H$ ($\gamma=2$) or not ($\gamma=1$), that is, whether the epigenetic change is elastic/inelastic. F is an asymmetric generalised normal distribution function, $F(S)=\Phi(y)$, with Φ the normal cumulative distribution function and y is defined as:

$$y(S;k,\Xi)=-\frac{1}{k}\log\left(1+\frac{S-\Xi}{\Xi}\right),$$

with $k<0$ the shape parameter and $\Xi>0$ the location parameter. This function is convenient since it has positive support (the oxygen level cannot be negative) and allows enough flexibility to consider different dependencies and the possibility of phenotype changes (or lack thereof) above S^H in a non-symmetric way.

The second, third and fourth terms in Eq. (10) correspond to the decay, inheritance and convection of the internal variable, respectively, as explained in Section 2.1, with Λ the decay rate and β the degree of phenotypic inheritance.

Regarding the effects of phenotypic changes in cell behaviour, we define the Ψ functions as beta distribution functions, which are bounded and therefore coherent with our definition of V as a bounded function. They also allow great flexibility for modelling different behaviours. In general, we write:

$$\Psi_i(V;a_i,b_i)=1+\frac{(V/V_{\max})^{a_i-1}(1-V/V_{\max})^{b_i-1}}{\mathrm{B}(a_i,b_i)},$$

with $i=\{\mathrm{mot},\mathrm{gr},\mathrm{d},\mathrm{u}\}$ and:

$$\mathrm{B}(a_i,b_i)=\frac{\Gamma(a_i)\Gamma(b_i)}{\Gamma(a_i+b_i)},$$

and Γ the Gamma function.

Model non-dimensionalisation. To simplify the interpretation of the *in silico* results, the model is reformulated in a dimensionless form, using the following dimensionless variables:

$$x=\frac{X}{L},\qquad t=TK_{\mathrm{gr}},\qquad c_i=\frac{C_i}{C_{\mathrm{sat}}}\ (i=\mathrm{a},\mathrm{d}),$$
$$v=\frac{V}{V_{\max}},\qquad s=\frac{S}{S^H},$$

where L is the length of the computational domain, $L=0.2\,\mathrm{cm}$. The value of the rest of the parameters used to define the dimensionless variables are $K_{\mathrm{gr}}=200\,\mathrm{h}$, $S^H=7\,\mathrm{mmHg}$, $C_{\mathrm{sat}}=5\cdot10^7\,\mathrm{cell/mL}$ (obtained from [55]) and $V_{\max}=1\,\mathrm{cell}^{-1}$ (arbitrarily set to define the V value corresponding to the CSC phenotype).

With such definitions, Eqs. (5), (6), (8), (10) can then be expressed as:

$$\frac{\partial c_{\mathrm{a}}}{\partial t}=\frac{\partial}{\partial x}\left(d_{\mathrm{c}}\frac{\partial c_{\mathrm{a}}}{\partial x}-m_{\mathrm{c}}c_{\mathrm{a}}\frac{\partial s}{\partial x}\right)+g_{\mathrm{c}}c_{\mathrm{a}}-n_{\mathrm{c}}c_{\mathrm{a}}, \tag{11}$$

$$\frac{\partial c_{\mathrm{d}}}{\partial t}=n_{\mathrm{c}}c_{\mathrm{a}}, \tag{12}$$

$$\frac{\partial s}{\partial t}=\frac{\partial}{\partial x}\left(d_s\frac{\partial s}{\partial x}\right)-g_s c_{\mathrm{a}}, \tag{13}$$

$$\frac{\partial v}{\partial t}=\omega-\lambda v+(\beta-1)f_{\mathrm{c}}v+\frac{1}{c_{\mathrm{a}}}\frac{\partial v}{\partial x}\left(d_{\mathrm{c}}\frac{\partial c_{\mathrm{a}}}{\partial x}-m_{\mathrm{c}}c_{\mathrm{a}}\frac{\partial s}{\partial x}\right), \tag{14}$$

with

$$d_{\mathrm{c}}=\kappa_{\mathrm{p}}\psi_{\mathrm{mot}}(v), \tag{15a}$$

$$m_{\mathrm{c}}=\kappa_{\mathrm{ch}}\pi_{\mathrm{ch}}(s)f_{\mathrm{sat}}(c_{\mathrm{a}})\psi_{\mathrm{mot}}(v), \tag{15b}$$

Table 1
Dimensionless parameters related with cell evolution.

Parameter	Value
κ_p	$9.0 \cdot 10^{-3}$
κ_{ch}	0.95
κ_d	0.24
κ_u	$5.1 \cdot 10^{3}$
κ_f	$1.6 \cdot 10^{3}$
s^A	0.23
Δs^A	$1.4 \cdot 10^{-2}$
s^M	0.36

The value of the parameters has been taken from [55] and are presented in their non-dimensional form.

$$g_c = \pi_{gr}(s) f_{sat}(c_a) \psi_{gr}(v), \tag{15c}$$

$$n_c = \kappa_d \pi_d(s) \psi_d(v), \tag{15d}$$

$$d_s = \kappa_f, \tag{15e}$$

$$g_s = \kappa_u \pi_u(s) \psi_u(v), \tag{15f}$$

$$\omega = \theta^+(1-v) + \theta^- v, \tag{15g}$$

$$\theta = \kappa_v(1 - \gamma F(s)), \tag{15h}$$

and the following dimensionless parameters:

$$\kappa_p = \frac{K_p}{L^2 K_{gr}}, \quad \kappa_{ch} = \frac{K_{ch} S^H}{L^2 K_{gr}}, \quad \kappa_d = \frac{K_d}{K_{gr}}, \quad \kappa_u = \frac{K_u C_{sat}}{S^H K_{gr}},$$

$$\kappa_f = \frac{K_f}{L^2 K_{gr}}, \quad \kappa_v = \frac{K_V}{K_{gr}}, \quad \lambda = \frac{\Lambda}{K_{gr}}.$$

The non-dimensional activation functions are expressed as:

$$\pi_{ch}(s) = \begin{cases} 1 - s & \text{if} \quad 0 \le s \le 1 \\ 0 & \text{if} \quad s > 1 \end{cases},$$

$$\pi_{gr}(s) = \begin{cases} s & \text{if} \quad 0 \le s \le 1 \\ 1 & \text{if} \quad s > 1 \end{cases},$$

$$\pi_d(s; s^A, \Delta s^A) = \frac{1}{2}\left(1 - \tanh\left(\frac{s - s^A}{\Delta s^A}\right)\right),$$

$$\pi_u(s; s^M) = \frac{s}{s + s^M},$$

$$f_{sat}(c_a, c_d) = 1 - \left(c_a + c_d\right),$$

$$\psi_i(v; a_i, b_i) = 1 + \frac{v^{a_i - 1}(1-v)^{b_i - 1}}{B(a_i, b_i)}, \quad i = \text{mot}, \text{gr}, \text{d}, \text{u},$$

with the parameters:

$$s^A = \frac{S^A}{S^H}, \quad \Delta s^A = \frac{\Delta S^A}{S^H}, \quad s^M = \frac{S^M}{S^H}, \quad \xi = \frac{\Xi}{S^H}.$$

The presented model has to be completed with suitable initial and boundary conditions.

Model parameters. As stated before, the parameters related to cell evolution are taken from a previous model [55]. The corresponding non-dimensional values are included in Table 1.

The value for the rest of the parameters is estimated within reasonable biological ranges and for illustrative purposes. In particular, the value of κ_v is set to 0.72 and the decay rate is assumed to be zero ($\lambda = 0$). The value of the parameters defining the function θ will be further explored in the next section. Regarding the parameters related to effect of the phenotype on cell behaviour, i.e., the parameters in the ψ functions, we define them to achieve functions consistent with biological evidence:

- Cells with a stem-phenotype have increased proliferation [60–63].
- Cells with a stem-like phenotype undergo the EMT and hence, increase their migratory activity [60,64].
- Stem cells are more resistant to apoptosis than differentiated cells and therefore, they present an overall lower death rate [65,66].
- Due to their increase in metabolic activity, cells with a stem-like phenotype consume more resources, and thus have a higher uptake rate [67].

Table 2
Value of the parameters defining the ψ functions.

Parameter	ψ_{mot}	ψ_{gr}	ψ_d	ψ_u
a	2	4	1.5	1.5
b	1	2	4	1

The parameters regulating how the state affects each phenomenon related to cell behaviour are presented.

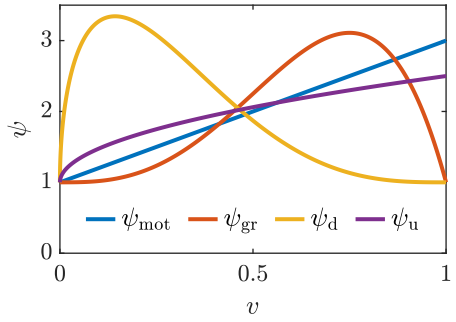

Fig. 1. Shape of the ψ functions for the different phenomena. ψ_{mot} and ψ_u are monotonically increasing functions; while ψ_{gr} and ψ_d are both non-monotonic, they increase, reach a maximum, and then decrease, reflecting that cells are most active in the phenotype corresponding to the maximum in the ψ function.

The precise values of the parameters is shown in Table 2 and the shape of the functions are presented in Fig. 1.

3. Results

In this section, we present the results obtained in different situations, to illustrate the model capacity to reproduce different trends in GBM evolution. First, in Section 3.1, an extensive parametric analysis is performed to analyse the effect of each parameter regulating the cell state evolution and to show the potential of the model for capturing different trends. Next, in Section 3.2, we study GBM evolution under different environmental conditions.

3.1. Model inspection

3.1.1. Model set-up

We investigate the effect of the different parameters involved in the evolution model of the internal variable (Eq. (14)) in a benchmark experiment of GBM evolution under cyclic hypoxia in microfluidic devices. Microfluidic techniques allow nowadays to reproduce, in a controlled microenvironment, the three-dimensional structure of tumours. In a previous work [55], a model of GBM evolution under hypoxia based on experiments on microfluidic devices was developed. In this work we continue to embrace this framework, since the recent development and advances in microfluidics enable the generation of large amounts of data which may be used for validation purposes.

The experimental configuration is one-dimensional, and recreates cells within the central chamber of a microfluidic device, of width L, with two lateral channels through which oxygen-rich medium can be perfused. This configuration simulates cells between two blood vessels in the brain, and allows controlling oxygenation conditions and creating oxygen gradients within the chamber. To subject cells to cyclic hypoxia, we simulate alternative oxygen perfusion through the channels, in cycles of $T = 7$ days ($t = 0.84$). A scheme of the device

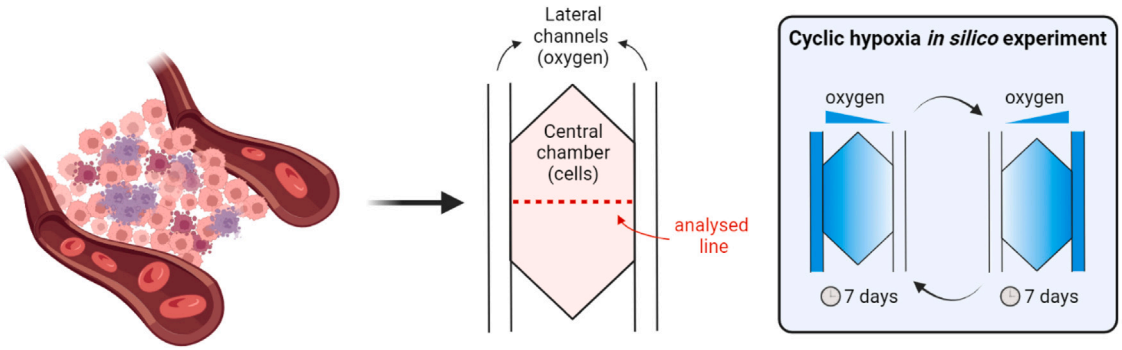

Fig. 2. Schematic representation of the microfluidic device and the experiment modelled. The microfluidic device reproduces the evolution of cancer cells between two blood vessels, which supply oxygen and nutrients. The experiment of cyclic hypoxia consists on perfusing oxygenated medium alternately through each channel while keeping the other one sealed, thus creating gradients. Created with BioRender.com.

configuration and our cyclic hypoxia *in silico* experiment are shown in Fig. 2.

The level of oxygen is above the hypoxic threshold in the oxygenated channel, $s = 9/7$, and below it in the non-oxygenated channel, $s = 1/7$. Consequently, we impose time-dependent Dirichlet boundary conditions for oxygen in both channels, with the corresponding value at each time point. The initial condition is set to be a straight line joining both channels, with constant gradient between the two boundary conditions. This is due to the quick oxygen diffusion, which causes the stationary profile to be reached in a short period of time, compared with the characteristic time of the cell processes considered.

Regarding alive cells, we assume that they are initially uniformly distributed within the chamber, at a low concentration $c_a(x, t = 0) = 0.08$ (far from the saturation limit). We assume that, initially, there are no dead cells ($c_d(x, t = 0) = 0$). Neither alive nor dead cells can go away from the chamber, so homogeneous Neumann boundary conditions are imposed for cells. The initial phenotypic state is uniform $v(x, t = 0) = v_0$ and, in order to explore its impact, it will be varied in each simulation.

We simulate 4 cycles of hypoxia, each with a duration of $t = 0.84$, yielding a total duration of the experiment of $t = 3.36$, corresponding to 28 days. The time step used for the computer simulations is $\Delta t = 0.0014$ (equivalent to 1000 s) and the element size for the spatial discretisation is $\Delta x = 0.005$ (equivalent to 10 μm). The system of partial differential equations (PDEs) is implemented in MATLAB and solved with the library `pdepe` [68].

To analyse the results, we introduce some metrics to represent the global macroscopic state of the tumour, aggregating spatial effects. First, we define the tumour burden (TB) as the total number of alive cells, as a measure of the size of the active tumour at each time:

$$\mathrm{TB}(t) = \int_0^1 c_a(x, t)\, \mathrm{d}x.$$

Analogously, we define the mean phenotypic state (MS) as the mean phenotype in the population at each point and time:

$$\mathrm{MS}(t) = \int_0^1 v(x, t)\, \mathrm{d}x.$$

3.1.2. Parametric analysis

First, in Fig. 3, we present a summary of simulations varying the parameters related with the evolution of the phenotypic state. Simulations have been performed and analysed for different values of the parameters that determine the function F, which establishes how the phenotypic state changes due to specific environmental conditions (in this case, due to the oxygen concentration). Also, we perform simulations for different values of the parameter β, which determines how cells inherit the phenotypic state of their progenitors. Finally, we have studied three different scenarios regarding the initial cell preconditioning, ranging from a tumour mainly composed of differentiated cells ($v_0 = 0.1$) to a tumour predominantly formed of CSCs ($v_0 = 0.9$). Details of these and other simulations, showing the whole temporal evolution of the TB and MS for the different parameters involved in the evolution of the phenotypic state, can be found in Appendix B.

From Fig. 3, it can been seen that different values of k and ξ lead to different global tumour dynamics, due to the nonlinear nature of the model. That is, the impact that the environment has on the phenotypic state of the tumour cells is determinant for the evolution of the tissue. In general, tumours with high ξ and k (in absolute value) evolve towards CSC phenotypes. Also, a low value of ξ generally translates into tumours made of differentiated cells. This is further explored in Figs. 4, 5. Besides, low initial preconditioning ($v_0 = 0.1$) facilitates the decrease in the number of alive cells.

Fig. 4 represents the simulation results for different values of ξ, leaving $k = -0.1$, $\beta = 1$ and $v_0 = 0.1$. ξ represents, somehow, the threshold determining if the cell's phenotype evolves towards a CSC phenotype ($s < \xi$) or towards a differentiated one ($s > \xi$). The higher the parameter ξ, the closer to CSC phenotype is the final phenotypic state. This is because a high value of ξ implies that cells are driven towards the CSC phenotype for a wider range of oxygen concentrations, that is, they are more sensitive to hypoxia.

Analogously, in Fig. 5 we can see simulations corresponding to different values of k, leaving $\xi = 1$, $\beta = 1$ and $v_0 = 0.1$. This parameter affects the spread of ω in the sense that higher absolute values of k lead to a smoother ω function, where cells are less sensitive to changes in the oxygen concentration. In particular, for $k = -10$ the cells' phenotype is almost insensitive to the oxygen concentration, so the phenotypic state is only slightly modified throughout the simulation. Indeed, in Fig. 3, we can observe that, in all the cases with $k = -10$, the final phenotypic state is similar to the initial one. For lower absolute values of k, the tumour is more aggressive in terms of velocities of proliferation and migration.

Phenotypic state inheritance also modifies the way the tumour evolves. Assuming $\beta = 0$ implies that cells, in some sense, repair the epigenetic changes caused by hypoxia through proliferation. At the other end, $\beta = 1$ implies that the population mean phenotypic state is preserved regardless of cell proliferation. From Fig. 3 it can be deduced that when the tumour is composed of differentiated cells (low v, greenish marker colours), tumour growth is favoured by no state inheritance ($\beta = 0$). Conversely, for tumours with a phenotypic state that is close to CSC, tumours with $\beta = 1$ grow more. There are even some cases where an intermediate state conservation by inheritance ($\beta = 0.67$) yields the tumours with the highest number of alive cells, which we can relate with a higher size of the active tumour. This can be explained by the hypotheses regarding the effect of the phenotypic state on cells via the ψ functions (see Fig. 1). For low values of v (phenotype of differentiated cells), overall tumour survival and growth is maximal for $v = 0$, since both death and uptake reach a minimum, compared with low $v \neq 0$, where death is at its peak. Thus, $\beta = 0$ helps achieving the $v = 0$ phenotype since, as commented above, it acts as a repair

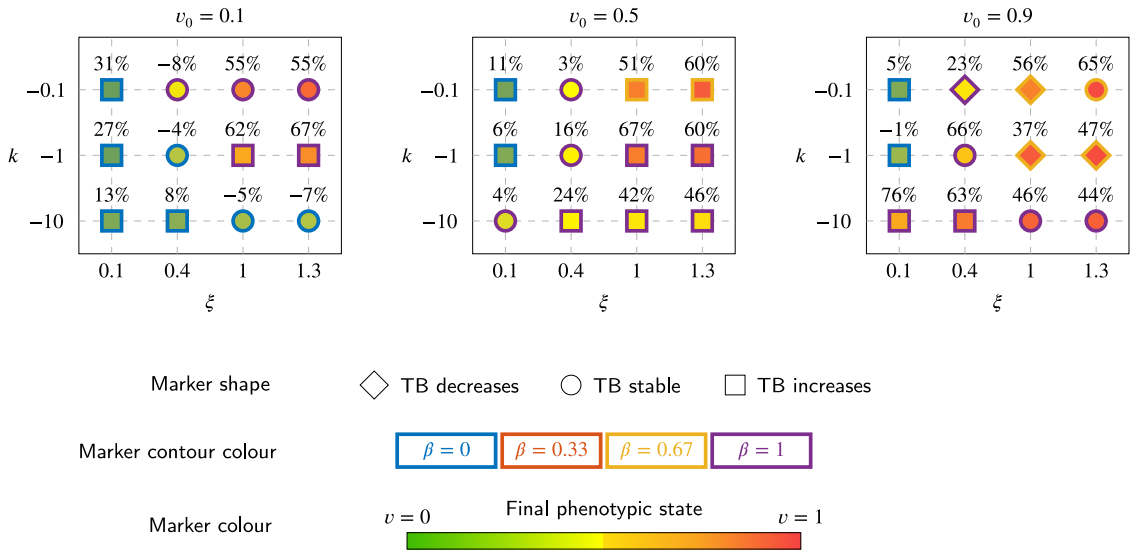

Fig. 3. Summary of simulations varying the parameters related with the phenotypic state evolution. Each diagram contains a grid of different shape-location parameters in function ω (modelling the acquisition-repair of epigenetic changes that lead to phenotypic plasticity), for a different initial preconditioning condition (that is, a different value of the initial phenotypic state v_0). The marker's shape determines the global trend of the number of cells in each simulation, that is, if the TB tends to increase, decrease or remains stable. The marker's contour colour represents which value of the inheritance parameter β favours the most tumour growth and, finally, the marker's inner colour shows the mean phenotypic state of the tumour cells at the end of the simulation. The percentage above each marker corresponds to the change in number of alive tumour cells during the simulation, when compared with the initial number.

process. Likewise, in the regime of CSCs (high values of v), the scenario promoting tumour growth coincides with the peak in ψ_{gr} ($v \approx 0.8$) and $\beta = 1$ helps cells achieving that range of phenotypic states. Since ψ_{gr} is not monotonic, there may be cases where a value of $\beta < 1$ helps getting the phenotype which best promotes tumour growth.

In Fig. 6 we analyse the effect of β for two different scenarios (I and II), corresponding to different behaviours, and also for different initial phenotypic states. Scenario I (Fig. 6(a)) corresponds to a case where cells barely change their phenotype. On the other hand, scenario II (Fig. 6(b)) corresponds to a case in which cells' phenotype is highly sensitive to changes in the oxygen concentration. Consequently, in the former, the phenotypic state mainly changes due to inheritance when cells proliferate while, in the latter, cells mainly evolve towards a CSC phenotype throughout successive cycles. In scenario I, with $v_0 = 0.1$, it can be observed that the tumour is within the differentiated cells regime, and therefore, as commented, $\beta = 0$ yields the biggest TB. In the other cases, cells have phenotypes closer to CSC and the value of β that produces the largest tumour is that yielding the closest value to $v \simeq 0.8$, that is, as pointed out before, the value that promotes tumour growth. However, in most cases the value of β does not modify the general progression pattern. The only exception is scenario I with $v_0 = 0.9$, where there are two differentiated trends, $\beta = 1$ produces a growing tumour with predominantly CSCs whereas $\beta < 1$ leads to TB reduction.

Next, we investigate the effect of different initial spatial distributions of the phenotypic state, that is, the effect of having cells distributed in different patterns according to their phenotype. In particular, we analyse four different distributions, all verifying that their mean state is $\int_0^1 v(x, t = 0)\,dx = 0.5$:

- uniform $v_0 = 0.5$,
- left-skewed: step-like distribution, with CSCs in the left ($v_0 = 0.9$) and differentiated cells in the right ($v_0 = 0.1$):

$$v(x, t = 0) = \begin{cases} 0.9 & \text{if} \quad x \leq 0.5 \\ 0.1 & \text{if} \quad x > 0.5 \end{cases},$$

- right-skewed: step-like distribution, with differentiated cells in the left ($v_0 = 0.1$) and CSCs in the right ($v_0 = 0.9$):

$$v(x, t = 0) = \begin{cases} 0.1 & \text{if} \quad x \leq 0.5 \\ 0.9 & \text{if} \quad x > 0.5 \end{cases},$$

Table 3
Summary of the different hypotheses regarding the effect of the internal variable in cell behaviour.

Scenario	Growth	Motility	Death	Uptake
Base	ψ_{gr}	ψ_{mot}	ψ_d	ψ_u
Effect only on growth	ψ_{gr}	1	1	1
No effect on growth	1	ψ_{mot}	ψ_d	ψ_u
No effect on uptake	ψ_{gr}	ψ_{mot}	ψ_d	1

The different hypotheses are translated into the activation/deactivation of the corresponding ψ function, a value of 1 means that the phenotypic state has no effect on that particular phenomenon.

- symmetric and non-uniform: logit-normal distribution with $\mu = 0$, $\sigma = 0.8$:

$$v(x, t = 0) = \frac{1}{2} \frac{1}{\sigma\sqrt{2\pi}} \frac{1}{x(1-x)} \exp\left(-\frac{(\text{logit}(x) - \mu)^2}{2\sigma^2}\right).$$

Figs. 7 and 8 show the results of TB and MS in two scenarios, for $\beta = 0$ and $\beta = 1$ respectively. In the first scenario, in both figures (Figs. 7(a), 8(a)), cells can withstand low levels of oxygen without acquiring stemness (the location parameter ξ is low), while the opposite occurs in scenario II (Figs. 7(b), 8(b)). Overall, it can be seen that although the spatial distribution of the phenotypic state is different in the early simulation times, this does not make a difference in the TB evolution or in the cell spatial distribution, neither qualitatively nor quantitatively. Only in Fig. 8(a) we can appreciate some differences, as an initial *step right* distribution yields a smaller tumour. Even in this case, differences are not significant, so we may conclude that the initial distribution of the phenotypic state does not affect tumour evolution in the long term.

To finish this study, we analyse the effect of modifying the hypotheses on the effect of the phenotypic state in cell behaviour, i.e., the definition of the ψ functions in the model. We compare the initial hypotheses defined in Section 2 (Fig. 1), which we consider the "base" condition, with a case in which hypoxia only modifies the proliferation capacity of cells, a scenario in which hypoxia modifies everything but the proliferation capacity, and a scenario in which it modifies everything but the oxygen uptake. A summary of these scenarios is presented in Table 3. The simulation results are presented in Fig. 9.

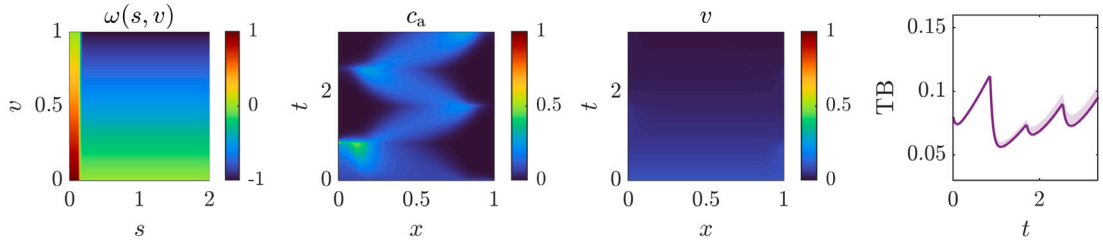

(a) $\xi = 0.1$.

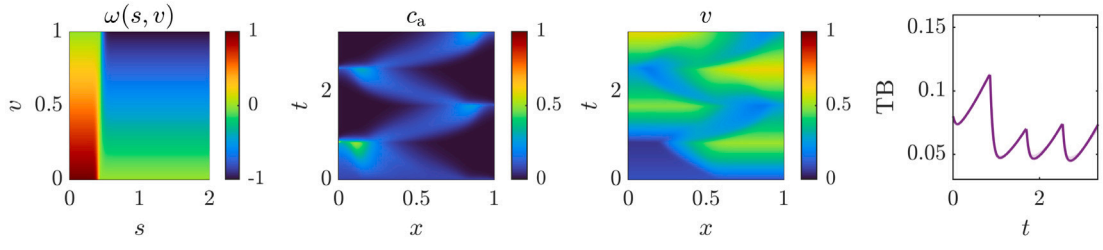

(b) $\xi = 0.4$.

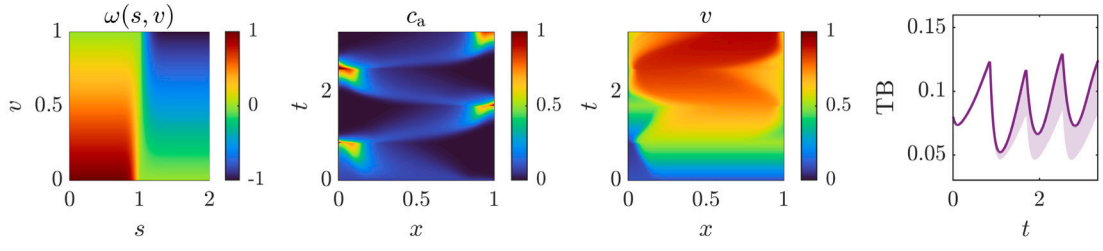

(c) $\xi = 1$.

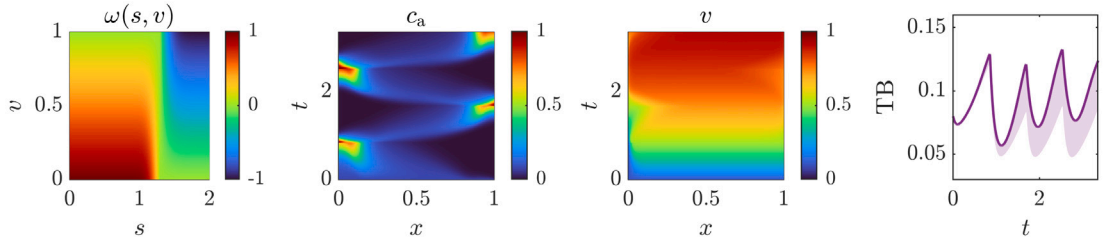

(d) $\xi = 1.3$.

Fig. 4. Effect of varying the location parameter ξ in function ω ($k = -0.1$). The first column represents ω as a function of oxygen s and the phenotypic state v. The second and third columns show the spatio-temporal dynamics of alive cells and the phenotypic state respectively. The fourth column shows the evolution of TB with respect to time, taking into account the variability induced by the inheritance parameter β (coloured region), with the solid purple line corresponding to the TB in the complete inheritance case $\beta = 1$.

From this figure, it can be seen that the effect of the phenotypic state on growth is essential to explain the different trends observed, since the assumption that there is no effect on growth leads to tumours that do not grow significantly. Indeed, the increase in growth is one of the defining features of CSCs [27]. On the other hand, considering that the change in phenotype is restricted only to the growth capability always yields bigger tumours. This is not a good representation of reality, since it would always lead to growing tumours (for example, in Fig. 9(a), it can be seen that the base hypothesis may lead to decreasing tumours, while considering only the effect on growth does not produce that trend). Besides, we know that the effect on motility (via the EMT) is also needed to characterise the transition towards CSCs. Finally, other authors have neglected the effect of phenotypic plasticity on oxygen uptake [39]. As can be seen in Fig. 9, this also leads invariably to big growing tumours. This hypothesis is not physiologically consistent as it fails to fulfil energetic constraints. That is, since cells have limited resources, an increase in their metabolic activity, either proliferative or migratory, must lead to an increase in uptake to fulfil the cell energy demands.

3.2. Study of GBM dynamics

In what follows we simulate GBM evolution under different oxygenation conditions. To simulate cyclic hypoxia, we define the (non-dimensional) oxygen concentration at the left (s_L) and right (s_R) edges of the domain with periodic boundary conditions in the form of sinusoidal functions, that can be parameterised by their period ($\mathcal{T}$), minimum level of oxygen ($s_{\min}$), amplitude (A) and phase-shift between both functions (ϕ):

$$s_L(t) = s_{\min} + A \sin\left(\frac{2\pi}{\mathcal{T}} t\right),$$

$$s_R(t) = s_{\min} + A \sin\left(\frac{2\pi}{\mathcal{T}} t + \phi\right).$$

We perform a sensitivity analysis to elucidate the effect of each of these four parameters on tumour evolution. We used latin hypercube

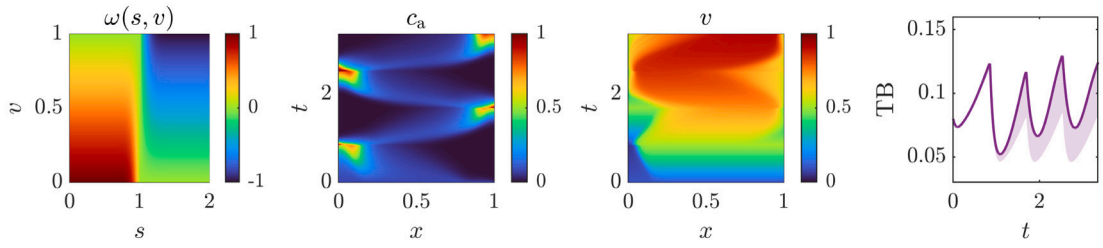

(a) $k = -0.1$.

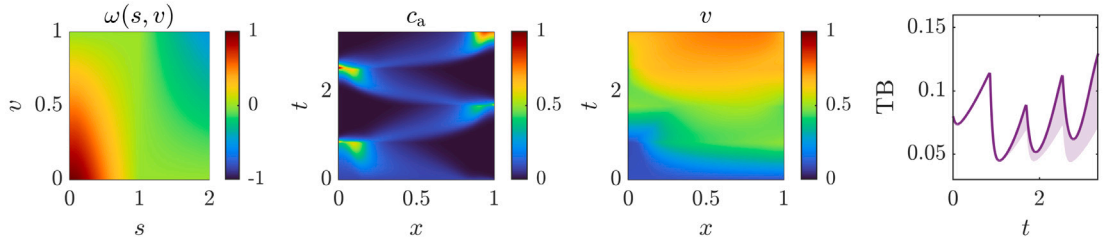

(b) $k = -1$.

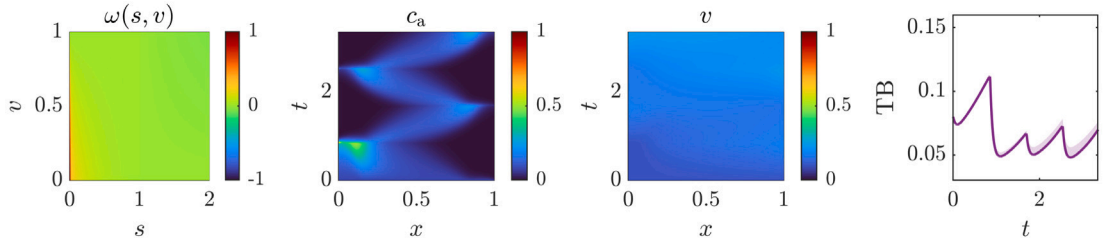

(c) $k = -10$.

Fig. 5. Effect of varying the shape parameter k in function ω ($\xi = 1$). The first column of figures represents ω as a function of oxygen s and the phenotypic state v. The second and third columns show the spatio-temporal dynamics of alive cells and the phenotypic state respectively. The fourth column shows the evolution of the TB with respect to time, taking into account the variability induced by the inheritance parameter β (coloured region), with the solid purple line corresponding to the TB in the complete inheritance case $\beta = 1$.

sampling to generate 300 combinations of the aforementioned parameters, with $0.12 \leq \mathcal{T} \leq 1.4$, $0 \leq s_{\min} \leq 1$, $0.14 \leq A \leq 1.14$, $0 \leq \phi \leq \pi$. Then, for each parameter combination, we simulate the tumour evolution for our two reference scenarios up to $t = 10$ and compute the partial correlation coefficients (PCCs) of each parameter with the TB at the end of the simulation. As observed in Fig. 10, in both scenarios, the period has no relevant correlation with the output value (final TB), while the TB has the highest correlation with the minimum value of oxygen $s_{\min}$.

In Fig. 11 we represent in a scatter plot the different simulations organised in terms of the values of $s_{\min}$, A and ϕ. The dot size is proportional to the period $\mathcal{T}$ (the bigger the dot, the higher the period in that simulation). As previously shown, $\mathcal{T}$ does not have a significant impact in the value of the final TB, so there is no particular pattern in the distribution of dot sizes in Fig. 11. We distinguish three global trends for the tumour burden: (i) the TB at the end is greater than at the beginning of the simulation (represented with a blue dot); (ii) the TB at the end is smaller than at the beginning of the simulation (represented with a yellow dot); (iii) the tumour has remitted at some point in the simulation (represented with an orange dot).

It can be seen that for both scenarios the results are similar. As shown by the PCCs, the parameter with the highest influence on TB dynamics is $s_{\min}$. Besides, lower values of the phase-shift increment the possibilities of tumour remission. In the limits, when $\phi \to 0$ there are times when the whole chamber is under hypoxic conditions, while when $\phi \to \pi$ there is always an oxygen gradient, with the more oxygenated area offering higher surviving possibilities.

Even if the results for both scenarios are alike in most cases, there are some remarkable differences, particularly for values of $s_{\min}$ under a certain threshold ($s_{\min} < 0.25$). Interestingly, insensitive tumours show a rate of extinction of 14%, while in the case sensitive this rate drops to 9%, suggesting that our model is able to capture the increased resilience that adaptation confers. To further study this, we calculate the surface defining the ranges of the parameters $s_{\min}$, A and ϕ that cause tumour remission. We use support vector machines (SVMs) with a polynomial kernel of order 2, since they provide an easy an efficient tool for nonlinear classifications [69]. The resulting surfaces are represented in Fig. 12, where it can be observed that the surface corresponding to insensitive tumours encloses a bigger area of remission. In particular, sensitive tumours seem to be able to withstand more severe hypoxia levels (lower values of $s_{\min}$), especially for higher amplitudes. A video showing the surfaces of Fig. 12 from different perspectives to allow an easier visualisation is included in the Supplementary Material.

Additional results showing the complete temporal evolution of the TB for some relevant parameter combinations can be found in Appendix B (Fig. 17). TB evolution shows that, in general, tumours that do not adapt in response to hypoxia (insensitive tumours) have a greater number of cells, i.e. a higher TB, than the ones that adapt. However, these latter survive longer, showing that even if the adaptive changes do not result in a higher TB, they provide an advantage for surviving in adverse environments.

4. Discussion

Throughout this paper, we have presented a new approach to modelling cellular adaptation and phenotypic plasticity in tumour evolution. This approach is based on incorporating internal variables to a

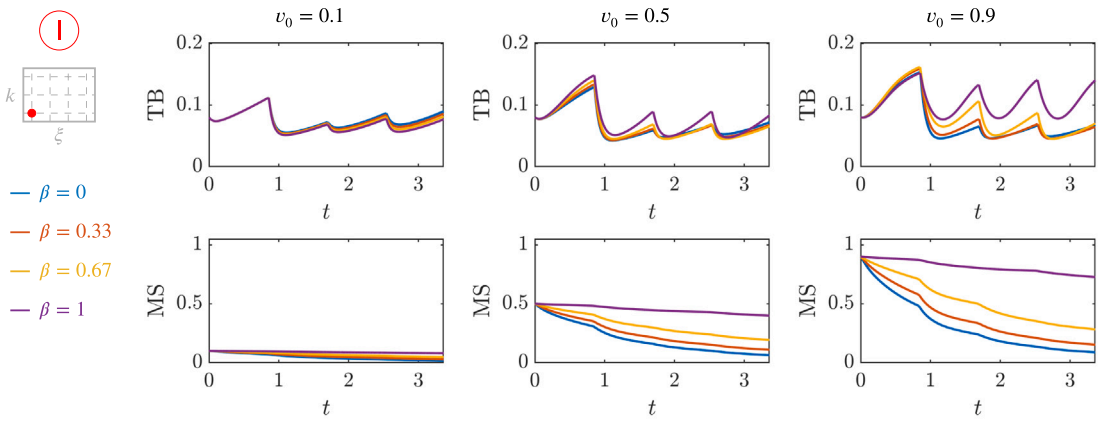

(a) Scenario I: $k = -10$, $\xi = 0.1$.

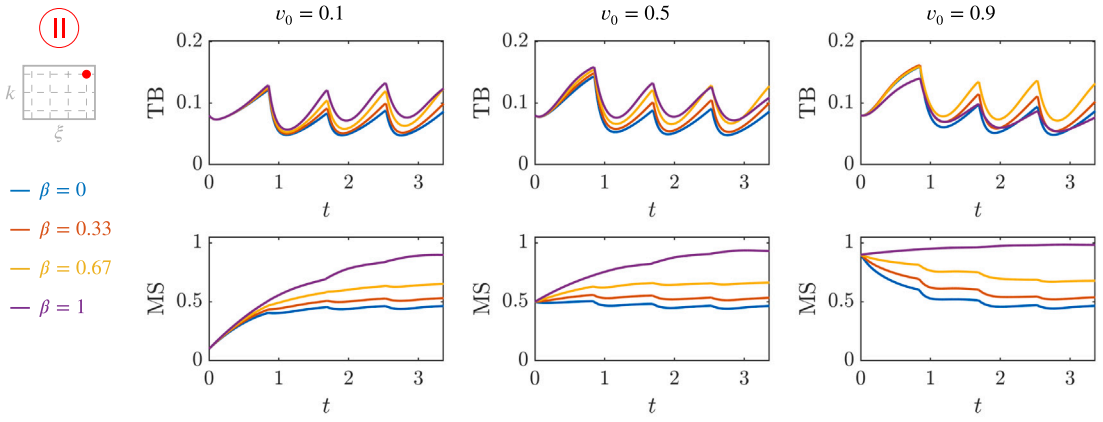

(b) Scenario II: $k = -0.1$, $\xi = 1.3$.

Fig. 6. Evolution of the TB (upper row in each subfigure) and the MS (lower row in each subfigure). Simulations consider different values of β and v_0, as well as two different combinations of (k, ξ) parameters.

previously defined continuum model. Here, internal variables fully describe cell state and its evolution representing, in a macroscopic sense, the molecular pathways that lead to changes in the cell's phenotype. In turn, cell state controls the response to external stimuli and overall cell behaviour.

A number of previous models tackle cell adaptation with continuum models from different perspectives. Models with a certain number of discrete phenotypes are the most widespread. In these models, each phenotype has a different behaviour (e.g., different proliferation or migration rate) usually represented by a differential equation, and cells switch from one phenotype to another with a certain transition rate, which is usually mediated by environmental conditions, such as the concentration of oxygen or a drug [38,40]. These models are simple to implement, because they only imply adding additional equations (one per phenotype), including phenotype transitions and changing the parameters; and they allow to reproduce some important tendencies. However, they do not reproduce the biological reality, where cells do not transition between discrete states, but undergo a range of different behaviours according to their gene expression, as have been shown for different cancers, such as colon [70] or lung [71]. Additionally, the number of parameters increases linearly with the number of different phenotypes considered, thus obscuring the fitting procedure and introducing numerical slack that may lead to overfitting.

There are also some approaches where cell phenotype is modelled using an artificial independent variable $d \in [0, d^{\max}]$ [37,39], representing the range of possible cell states, that is, adding an extra dimension to the problem (we will refer to this approach as *external dimension approach*, in opposition to our *internal variable approach*). This method overcomes the aforementioned limitation of discrete-phenotype models. Also, it does not require additional equations, but only the inclusion of flux terms on dimension d to account for cell state transitions. Besides, this approach allows obtaining the phenotype spatial distribution at each time point. However, it may be necessary at some point to include different internal variables, due to, for example, different scales for different epigenetic processes, such as the response to hypoxia and to a drug. In the external dimension approach, this implies adding extra dimensions, whose interpretation and implementation may be cumbersome, requiring discretisation in higher dimension spaces. This leads to increases in the computational cost of the simulations, giving rise to the so-called curse of dimensionality.

The work by Lei et al. [72] presents another approach to cell adaptation that also takes into account the distribution of phenotypic states at each point, on this occasion for the case of stem cell regeneration. However, the model does not use differential equations but integral equations to evaluate cell number at each time point (there is no spatial coordinate). The model also lacks the relationship between the environment and the phenotype, with cells acquiring epigenetic changes randomly, even if it does consider the inheritance of such states.

The model presented in this paper describes phenotype as a continuum field, but instead of representing it as an extra dimension, we use internal variables to describe it. To the authors' knowledge, this is the first model in cell evolution taking this approach, which is otherwise widely used in other disciplines, such as damage [47,73,74] or control theory [46]. This approach requires defining an evolution equation for the internal variables, which in our case takes the form of

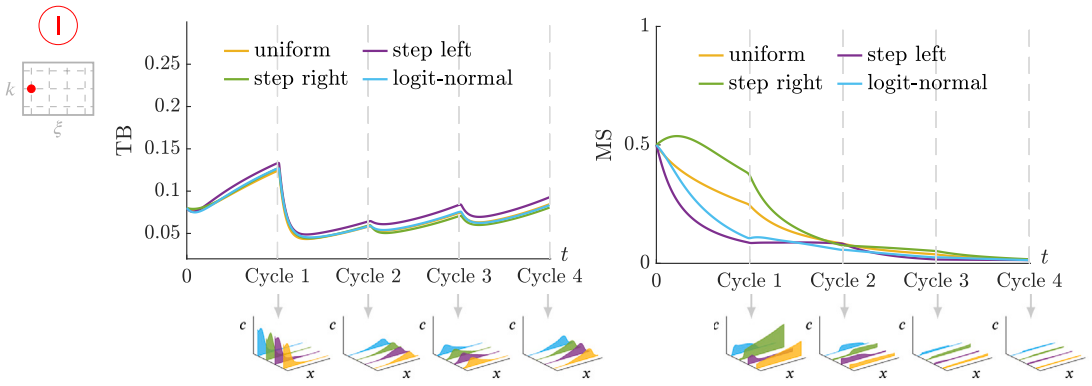

(a) Scenario I: $k = -1$, $\xi = 0.1$.

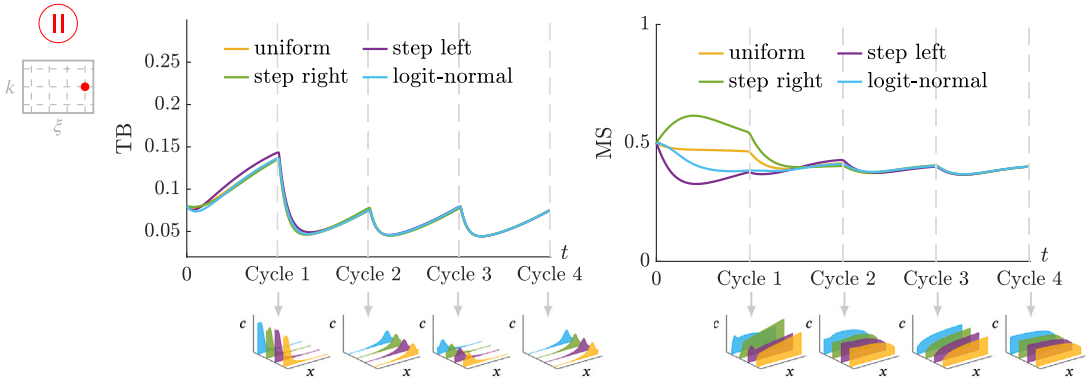

(b) Scenario II: $k = -1$, $\xi = 1.3$.

Fig. 7. Effect of the initial distribution of cells according to their phenotype on tumour evolution, for the two different scenarios and no inheritance. Scenario I corresponds to cell phenotype insensitive to oxygen variations ($k = -1$, $\xi = 0.1$), and scenario II to cell phenotype insensitive to oxygen variations ($k = -1, \xi = 1.3$). The TB and MS are represented for each scenario, together with the spatial distributions of c_a and v at the end of each cycle.

another transport equation. State internal variables have been mostly used in Lagrangian frameworks, whereas we introduce them within an Eulerian one. This requires incorporating convective terms, inherent to Eulerian frameworks, to enable cells to keep their state. This feature represents another aspect of novelty of this paper. The definition of the transport equation for cell phenotype is straightforward from the biological hypotheses, allowing to include source terms directly relating stimuli and cell state. This may represent an advantage with respect to the external dimension approach, where interpretability is somehow hindered and of course, with respect to [72], where there is no relationship between state and environment, something crucial for cellular adaptation. In contrast to [72], our model also incorporates the spatial coordinate to account for cell migration, especially relevant for tumour invasion. Finally, sticking to the numerical complexity of the model, including additional internal variables in our model (only) implies adding equations, overcoming the drawbacks related to the computational cost mentioned for the external dimension approach [39]. Also in this regard, it requires less parameters than discrete phenotype models, yielding simpler models, easier to implement, calibrate and validate.

However, the proposed model also presents limitations, since it can only provide the mean phenotypic state at each spatial point, whereas both the external dimension model [39] as well as the integral model with random epigenetic changes [72] allow to get the phenotypic distribution at each point. In this sense, our model offers a simplified representation of the models taking into account the phenotypic state distribution [39,72], and can be seen as a result of averaging the distribution of states at each point. The mathematical relationship between these two different approaches could be further explored.

In summary, the presented framework permits simulating the interplay between cell behaviour and the environment, through the concept of cell state. The framework is general and the formulation introduced in Section 2.1 can be adapted to different biological problems, with different cell populations, chemical species, and other type of external signals in the microenvironment as well as different internal variables. Of course, each problem would require to define particular biologically-adapted correction functions with their associated parameters. In the model, the cell state has a unique value at each point. Hence, we lose the state distribution in a local point, but we assume that, at the population level, working with averaged values representing the collective behaviour is a reasonable simplification.

Besides, there are some other limitations related to the validation of the model. As previously said, the model for GBM evolution that is used as a starting point has already been validated with different experiments in microfluidic devices [38,55,75] However, the extension presented here for describing cell adaptation has yet to be experimentally validated. To endow this model with predictive capacity, validating it with experimental data is paramount. Nevertheless, the required experiments are cumbersome and present some important technical difficulties. For example, the cyclic hypoxia experiment in a microfluidic device used here as benchmark requires the ability of opening and closing the channels of the device, and ideally some way of measuring the epigenetic changes that take place, even if qualitatively. Hopefully, microfluidics is a field in constant and rapid evolution, and new techniques are emerging to measure epigenetic marks and gene expression via, for example, RNA sequencing [76,77].

As a first approach to get a deeper insight on the performance of the model and to compare with actual biological known facts, we have presented here several illustrative examples with a thorough parametric analysis. The objective of this study was to analyse the potential of the model for capturing important biological trends. Indeed, the results here presented reproduce some trends that have been reported in the existing literature about CSCs, GBM and cyclic hypoxia. It has

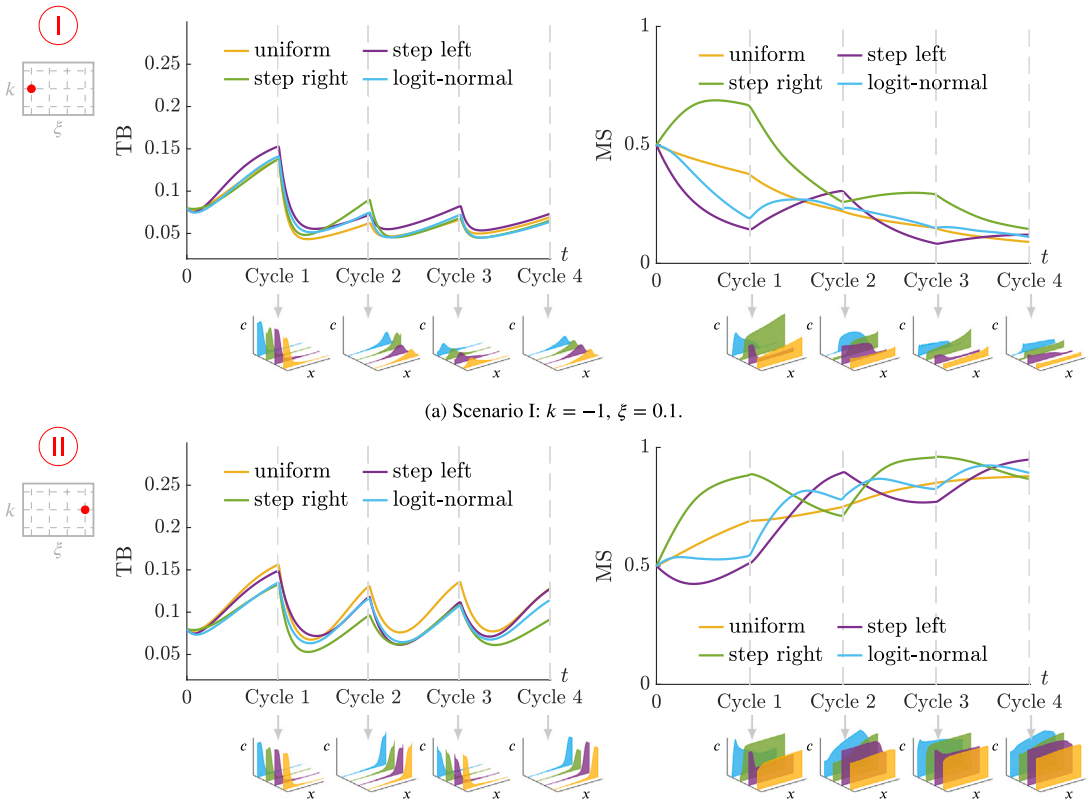

(a) Scenario I: $k = -1$, $\xi = 0.1$.

(b) Scenario II: $k = -1$, $\xi = 1.3$.

Fig. 8. Effect of the initial distribution of cells according to their phenotype on tumour evolution, for the two different scenarios and complete inheritance. Scenario I corresponds to cell phenotype insensitive to oxygen variations ($k = -1$, $\xi = 0.1$), and scenario II to cell phenotype insensitive to oxygen variations ($k = -1, \xi = 1.3$). The TB and MS are represented for each scenario, together with the spatial distributions of c_a and v at the end of each cycle.

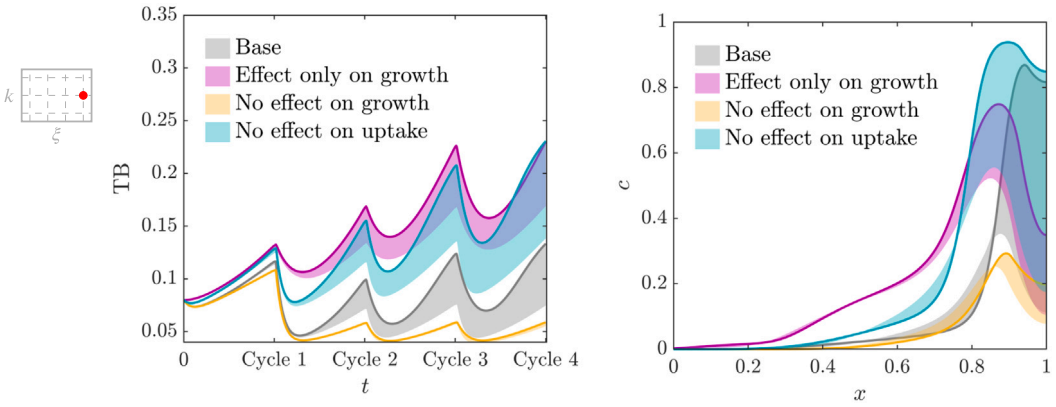

(a) Tumour Burden (TB) evolution.

(b) Cell concentration profile at final time.

Fig. 9. Effect of different hypotheses about the effect of the internal variable in cell behaviour. The results are presented for a moderately sensitive tumour ($k = -1$, $\xi = 1.3$) initially composed of differentiated cells ($v_0 = 0.1$). The coloured band represents tumour evolution taking into account all possible β values, with the solid line corresponding to the simulation with $\beta = 1$.

been reported that the most aggressive tumours contain the highest number of CSCs [62], which is in line with the results shown in Fig. 3 where tumours that initially have a higher proportion of CSCs grow more. The model allows obtaining different global trends of tumour evolution depending on the parameters regulating phenotype changes, which reinforces the idea that epigenetic events are behind tumour heterogeneity [29,78]. Moreover, with this model, different hypotheses regarding the effect of phenotypic changes caused by hypoxia on cell behaviour can be tested, and it has been shown that the effects on growth and oxygen uptake are particularly relevant if we want to reproduce GBM aggressiveness (see Fig. 9). This conclusion is in agreement with previous findings, proving that increased growth [63] and consumption [79] are defining features of these cells. Besides, investigating the effect of cyclic hypoxia, we have shown that cells that undergo phenotypic changes to adapt show increased resilience in hypoxic environments (Figs. 11, 12). The use of an experiment recreating cyclic hypoxia is supported by the fact that it is a relevant phenomenon occurring inside most tumours due to their aberrant vasculature [80], and yielding more aggressive tumours than chronic hypoxia (Fig. 17) [81].

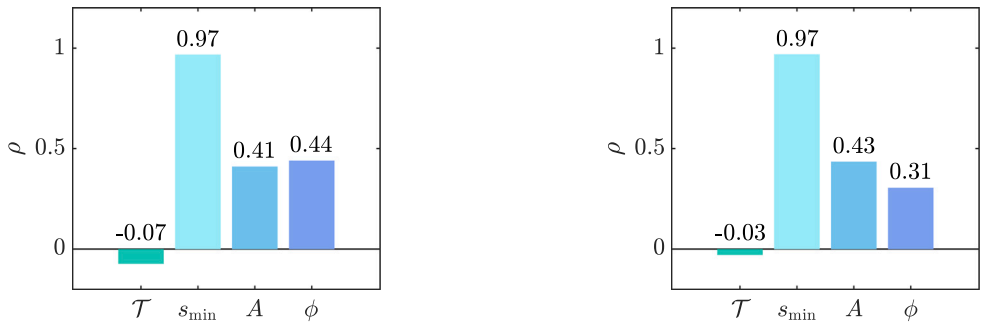

(a) Scenario I. (b) Scenario II.

Fig. 10. Partial correlation coefficients relating the parameters defining oxygen boundary conditions to the final tumour burden. Scenario I corresponds to cells whose phenotype is quite insensitive to oxygen variation, while in scenario II, the cells' phenotype is sensitive to changes in oxygen concentration.

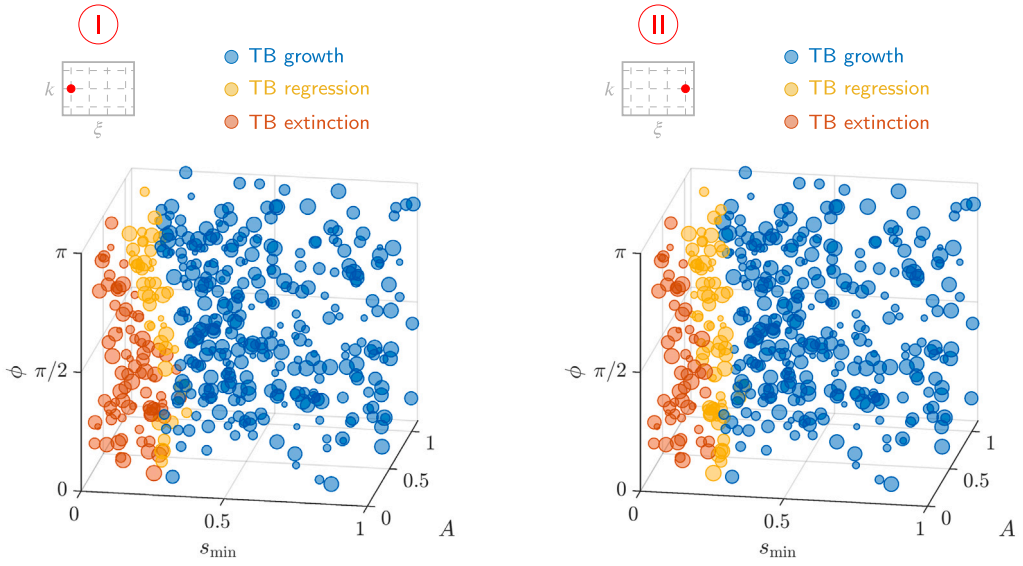

(a) Scenario I: Phenotype insensitive to oxygen variations. (b) Scenario I: Phenotype sensitive to oxygen variations.

Fig. 11. Scatter plot of the outcome of the simulations in terms of $s_{\min}$, A and ϕ. A blue dot indicates that the TB has grown, a yellow dot indicates that it has diminished, and an orange dot indicates that the tumour has become extinct. The dot size is proportional to the period $\mathcal{T}$ so that bigger dots correspond to simulations with a higher period.

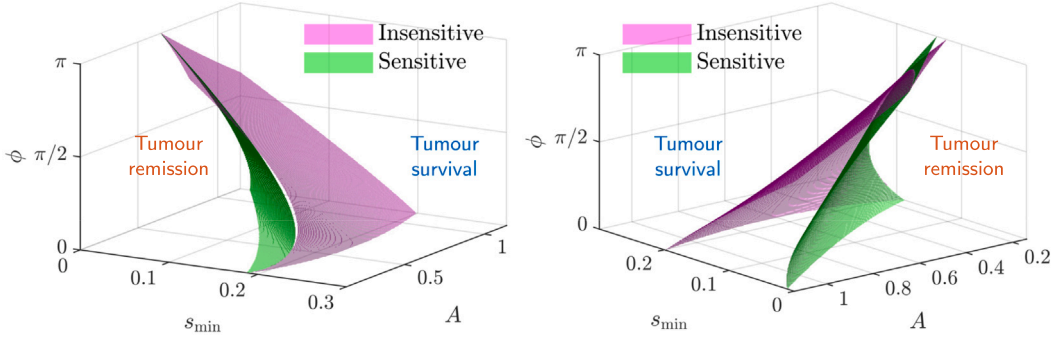

Fig. 12. Surface separating tumour remission and tumour survival. This surface has been calculated for sensitive (green) and insensitive (pink) populations using SVM with a polynomial kernel of order 2. Two different perspectives are depicted to facilitate visualisation.

Finally, one-dimensional simulations are carried out as proof of concept of the model, due to its easy implementation and reduced computational cost, but they also imply some limitations. Moreover, the proposed *in silico* experiment, consisting on back and forth migration within the chamber, does not correspond exactly with what happens in the brain, where the tumour has no space constraint and expands. Therefore, the application of this model to real patient-specific geometries is an interesting line to explore in the future.

In spite of these limitations, mathematical models, and in particular the one presented here to model epigenetic changes in cell populations as well as the associated effect on the behaviour of the population, are really useful for understanding biological phenomena. Our model is

able to reproduce different trends reported in literature. Of course there is room for improvement, and the validation of the model together with the generalisation to more dimensions and internal variables should be addressed in the future. For example, the inclusion of an internal variable taking into account the phenotypic changes that take place in response to chemotherapy treatments could be interesting, given that there are studies suggesting that drug resistance is favoured by hypoxia [82].

5. Conclusion

Cellular adaptation mediated by epigenetic changes and leading to phenotypic heterogeneity is a major concern in cancer research since it has proven to be determinant in the tumour aggressiveness, and hence, in its prognosis, to the extent that it was included as a Cancer Hallmark in 2022.

In this paper, we have presented a novel approach for modelling these phenomena based on reaction–diffusion equations with internal variables modelling the cell state. This model has been formulated in general, and then particularised to the case of glioblastoma adaptation to hypoxia. Hypoxia promotes the development of cancer stem cells which have increased proliferation and migration rates and are responsible for the dismal prognosis of this tumour.

The main features of the model, such as the acquisition of phenotypic changes, its inheritance and the effect of plasticity in cell behaviour have been analysed by means of an extensive parametric analysis showing the model's flexibility and capability to get relevant physiological results that capture the huge variability present in tumours. Indeed, it is able to reproduce growing, stable or decreasing tumours, depending on the sensitivity of the cells to changes in their microenvironment and without particular trends, showing the non linearity of the model and the hidden dependencies. We emphasise the importance of taking into account the effect of adaptation to hypoxia in proliferation, because otherwise we are not able to capture the increased aggressiveness observed in literature in tumours subjected to cyclic hypoxia. Besides, the increased consumption caused by phenotypic changes leading to cancer stem cells is also important not to overestimate growth of tumours, neglecting the energetic constraints.

Finally, a study on tumour dynamics, when varying the boundary conditions for oxygen concentrations has been carried out, showing that incorporating cellular adaptation results in an increased resilience of glioblastoma tumours. Indeed, tumours that undergo phenotypic changes are less likely to remit.

The presented framework takes a further step towards creating models that are able to reproduce the complexity of this disease and provide predictive tools to *in silico* test different treatments and conditions.

CRediT authorship contribution statement

Marina Pérez-Aliacar: Conceptualization, Methodology, Software, Formal analysis, Visualization, Writing – original draft, Writing – review & editing. **Jacobo Ayensa-Jiménez:** Conceptualization, Methodology, Software, Formal analysis, Writing – review & editing, Supervision. **Manuel Doblaré:** Conceptualization of this study, Methodology, Writing – review & editing, Supervision, Project administration, Funding acquisition.

Declaration of competing interest

None declared

Acknowledgements

The authors gratefully acknowledge the financial support from the Spanish Ministry of Science and Innovation (MICINN), the State Research Agency (AEI), Spain, through the project PID2021-126051OB-C41.

Appendix A. Derivation of the evolution equations.

The main equations of the mathematical models presented throughout this paper are differential conservation equations, which are derived from their integral form.

A.1. Cells and chemical species

Let us suppose that we have m cell populations whose concentration is C_i, and n chemical species with concentration S_i. We may define a vector $\boldsymbol{U}$ formed by all the $m+n$ solution variables as:

$$\boldsymbol{U} = [C_1, \dots, C_m, S_1, \dots, S_n], \quad i = 1, \dots, n+m. \tag{16}$$

The integral conservation law for any of the variables defined per unit volume may be written as:

$$\frac{\mathrm{d}}{\mathrm{d}t}\int_{\mathcal{V}} U_i \,\mathrm{d}v = -\oint_{\partial\mathcal{V}} \boldsymbol{q}_i \cdot \mathrm{d}\boldsymbol{S} + \int_{\mathcal{V}} F_i \,\mathrm{d}v, \tag{17}$$

where $\boldsymbol{q}_i$ stands for the flux of cells/chemical species that goes through the surface of the control volume $\mathcal{V}$, and F_i represents the source term in each time per unit volume.

Applying the divergence theorem, we get:

$$\frac{\mathrm{d}}{\mathrm{d}t}\int_{\mathcal{V}} U_i \,\mathrm{d}v = -\int_{\mathcal{V}} \boldsymbol{\nabla}\cdot\boldsymbol{q}_i \,\mathrm{d}v + \int_{\mathcal{V}} F_i \,\mathrm{d}v, \tag{18}$$

from where we can obtain, for an arbitrary volume $\mathcal{V}$:

$$\int_{\mathcal{V}} \left(\frac{\partial U_i}{\partial t} + \boldsymbol{\nabla}\cdot\boldsymbol{q}_i - F_i\right)\mathrm{d}v = 0, \tag{19}$$

so finally we derive the differential conservation equation:

$$\frac{\partial U_i}{\partial t} = -\boldsymbol{\nabla}\cdot\boldsymbol{q}_i + F_i, \tag{20}$$

which constitute the system of governing equations in the presented model.

The source term for cells F_i $(i = 1, \dots, m)$, which will be needed for the derivation of the governing equation for internal variables, comprises the terms of cell proliferation and death, and can be expressed as:

$$F_i = U_i(f_i - d_i). \tag{21}$$

A.2. Internal variables

To derive the evolution equation for internal variables, the starting point is the conservation law for the total amount of variable in a RVE.

Let V_{ik} be the k^{th} internal variable affecting the i^{th} cell population, whose associated field variable is the cell concentration U_i $(i = 1, \dots, m)$. Therefore, the total amount of internal variable per unit volume is expressed as $U_i V_{ik}$ and its integral balance equation is:

$$\frac{\mathrm{d}}{\mathrm{d}t}\int_{\mathcal{V}} U_i V_{ik} \,\mathrm{d}v = -\oint_{\partial\mathcal{V}} V_{ik}\boldsymbol{q}_i \cdot \mathrm{d}\boldsymbol{S} + \int_{\mathcal{V}} R_{ik} \,\mathrm{d}v, \tag{22}$$

$$i = 1, \dots, m; \quad k = 1, \dots, r_i. \tag{23}$$

where r_i is the number of internal variables affecting the i^{th} population. The first term of the RHS represents the amount of internal variable going in or out of the volume $\mathcal{V}$ due to the effect of the cell flux $\boldsymbol{q}_i$, and the second term is the source term.

Applying the divergence theorem to the surface integral:

$$\frac{\mathrm{d}}{\mathrm{d}t}\int_{\mathcal{V}} U_i V_{ik} \,\mathrm{d}v = -\int_{\mathcal{V}} \boldsymbol{\nabla}\cdot(V_{ik}\boldsymbol{q}_i) \,\mathrm{d}v + \int_{\mathcal{V}} R_{ik} \,\mathrm{d}v. \tag{24}$$

Letting the temporal derivative inside the integral in the LHS and subsequently grouping the integrals, we obtain:

$$\frac{\partial(U_i V_{ik})}{\partial t} = -\boldsymbol{\nabla}\cdot(V_{ik}\boldsymbol{q}_i) + R_{ik}. \tag{25}$$

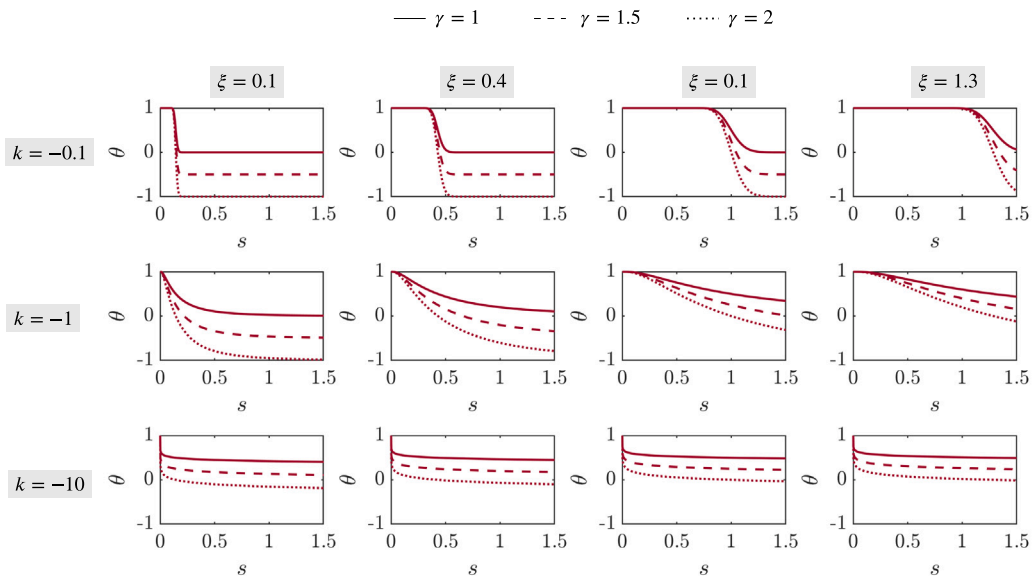

Fig. 13. Different shapes of function θ. Simulations are performed for different values of the parameters defining function θ. In particular, the location parameter in function θ increases from left to right, and the shape parameter k increases from bottom to top. In each subfigure, functions with different values of the repair parameter γ are plotted with different line styles ($\gamma = 1$ with a continuous line, $\gamma = 1.5$ with a discontinuous line and $\gamma = 2$ with a dotted line).

Then, applying the product rule:

$$U_i \frac{\partial V_{ik}}{\partial t} + V_{ik} \frac{\partial U_i}{\partial t} = -V_{ik} \nabla \cdot \boldsymbol{q}_i - \boldsymbol{q}_i \cdot \nabla V_{ik} + R_{ik}. \tag{26}$$

and using Eq. (20):

$$U_i \frac{\partial V_{ik}}{\partial t} + V_{ik} \left(-\nabla \cdot \boldsymbol{q}_i + F_i\right) = -V_{ik} \nabla \cdot \boldsymbol{q}_i - \boldsymbol{q}_i \cdot \nabla V_{ik} + R_{ik}. \tag{27}$$

Reorganising and simplifying the previous equation, we arrive to a differential equation for the evolution of the internal variables:

$$U_i \frac{\partial V_{ik}}{\partial t} = -\boldsymbol{q}_i \cdot \nabla V_{ik} + R_{ik} - V_{ik} F_i, \tag{28}$$

where we can introduce the expression for F_i defined in Eq. (21):

$$U_i \frac{\partial V_{ik}}{\partial t} = -\boldsymbol{q}_i \cdot \nabla V_{ik} + R_{ik} - V_{ik} U_i (f_i - d_i), \tag{29}$$

In Eq. (29) it remains to be defined the source term for the internal variables R_{ik}, defining the amount of V_{ik} that is generated or disappears at each time moment. R_{ik} is presented as a sum of different terms $R_{ik} = \sum_n R^n_{ik}$, comprising the following phenomena:

- R^1_{ik}: Internal variable accumulation due to external effects. One of the main hypothesis of this framework is that the phenotypic state of a cell and its associated behaviour depend on the history of external stimuli to which the cell has been subjected. Therefore, the internal variable representing this state depends on those external stimuli through function Ω_{ik}, which may depend on $S_1, \dots, S_n$, and other microenvironmental signals. With these assumptions, the corresponding term is written as:

$$R^1_{ik} = \Omega_{ik} U_i. \tag{30}$$

- R^2_{ik}: Cell repair. In general, we assume that epigenetic changes, that lead to the accumulation of internal variables and to the change of cell behaviour, are reversible and that cells can repair themselves through diverse pathways [49–51]. Thereupon, we include a decay term:

$$R^2_{ik} = -\Lambda_{ik} U_i V_{ik}, \tag{31}$$

with λ_{ik} the decay rate.

- R^3_{ik}: Inheritance. Daughter cells may inherit the epigenetic changes acquired by their progenitors [52–54] in a proportion $\beta_{ik} \in [0, 1]$, so that if $\beta_{ik} = 1$, daughter cells are identical to their progenitors and they have the same phenotypic state, and if $\beta_{ik} < 1$, daughter cells do not inherit all the epigenetic changes. The corresponding term is written as:

$$R^3_{ik} = \beta_{ik} f_i U_i V_{ik}, \tag{32}$$

where f_i is the cells growth term.

- R^4_{ik}: Decrease due to death. When cells die, the total amount of internal variable inside a volume diminishes at rate d_i, so we can write:

$$R^4_{ik} = -d_i U_i V_{ik}. \tag{33}$$

Once all the terms have been defined, we can substitute R_{ik} in Eq. (29) and simplify terms, obtaining the general transport equation for internal variables V_{ik}:

$$\frac{\partial V_{ik}}{\partial t} = \frac{1}{U_i} \left(-\boldsymbol{q}_i \cdot \nabla V_{ik}\right) + \Omega_{ik} - \Lambda_{ik} V_{ik} + (\beta_{ik} - 1) f_i V_{ik}, \tag{34}$$

$$i = 1, \dots, n, k = 1, \dots, r_i. \tag{35}$$

Appendix B. Details of parametric analyses

B.1. Model parameters

In this section we present an extended study of the parameters defining the acquisition of phenotypic changes, mediated by function θ:

$$\theta = \kappa_v (1 - \gamma F(s; k, \xi)),$$
$$F(s) = \Phi(y),$$
$$y(s; k, \xi) = -\frac{1}{k} \log\left(1 + \frac{s - \xi}{\xi}\right).$$

First, in Fig. 13 we present the effect of the different parameters on the shape of the function. Specifically, ξ is a location parameter

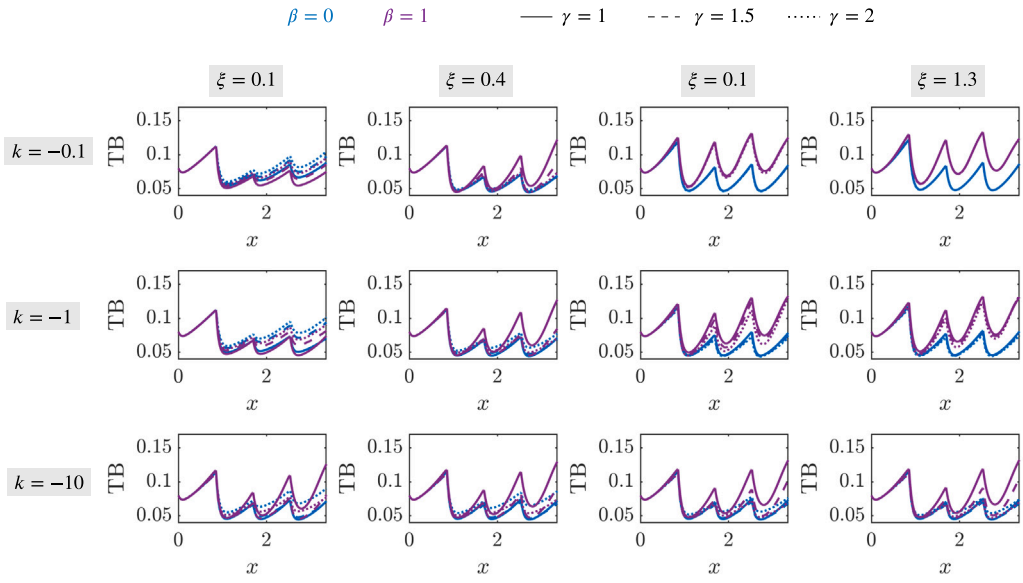

(a) Evolution of the TB.

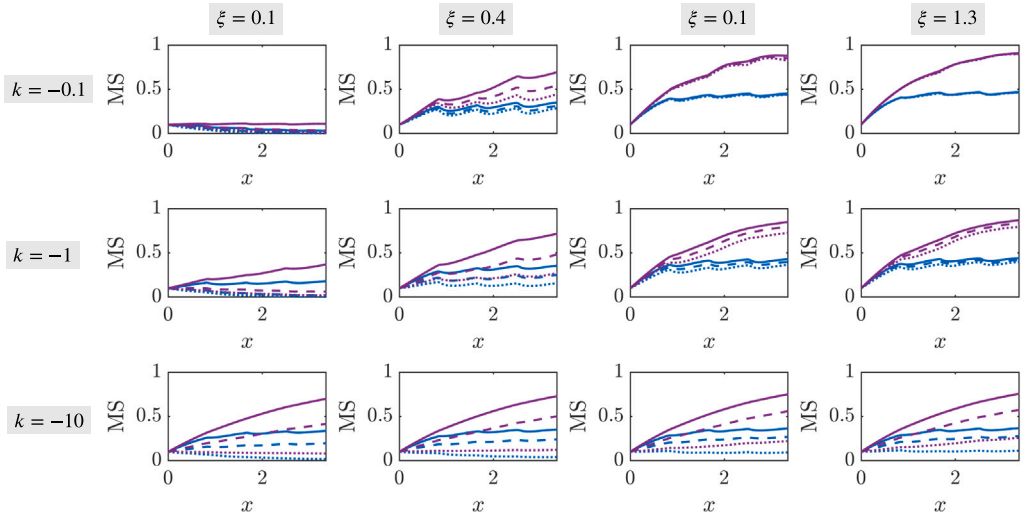

(b) Evolution of the MS.

Fig. 14. Evolution of TB and MS for an initial phenotypic state $v_0 = 0.1$. The grid shows simulations with different parameters related to the evolution of the phenotypic state. In particular, the location parameter in function ω increases from left to right, and the shape parameter k increases from bottom to top. In each subfigure, simulations for two different β values are plotted with different colours ($\beta = 0$ in blue and $\beta = 1$ in purple) and different values of the repair parameter γ are plotted with different line styles ($\gamma = 1$ with a continuous line, $\gamma = 1.5$ with a discontinuous line and $\gamma = 2$ with a dotted line).

and specifies the level of oxygen below which cells undergo phenotypic changes towards a cancer stem cell phenotype. k is a shape parameter defining the spread of the function and finally, $\gamma \in [1, 2]$ is a parameter setting whether cells differentiate again when the oxygen concentration is above ξ, that is, if epigenetic changes are elastic/inelastic. If $\gamma = 1$, cells do not experiment any phenotypic changes when exposed to high levels of oxygen (inelastic behaviour), while if $\gamma = 2$, cells move towards differentiated phenotypes for high oxygen concentrations (elastic behaviour).

In Figs. 14–16 we show the evolution of the TB and the MS for the different functions θ depicted in Fig. 13 and for different initial phenotypic states.

B.2. Environmental parameters related to the oxygenation conditions

Here we present some illustrative results of TB evolution in different oxygenation conditions, parameterised in terms of $\mathcal{T}$, $s_{\min}$, A and ϕ. As shown by the PCCs (Fig. 10), $\mathcal{T}$ has no significant impact in the final value of the TB. Hence, we represent its variability with a band for each combination of $s_{\min}$, A and ϕ.

Table 4 presents twelve representative combinations of those three parameters, together with the observed trend in the TB (growth, regression or extinction). The temporal evolution of the TB for each of the twelve configurations mentioned in Table 4 is represented in

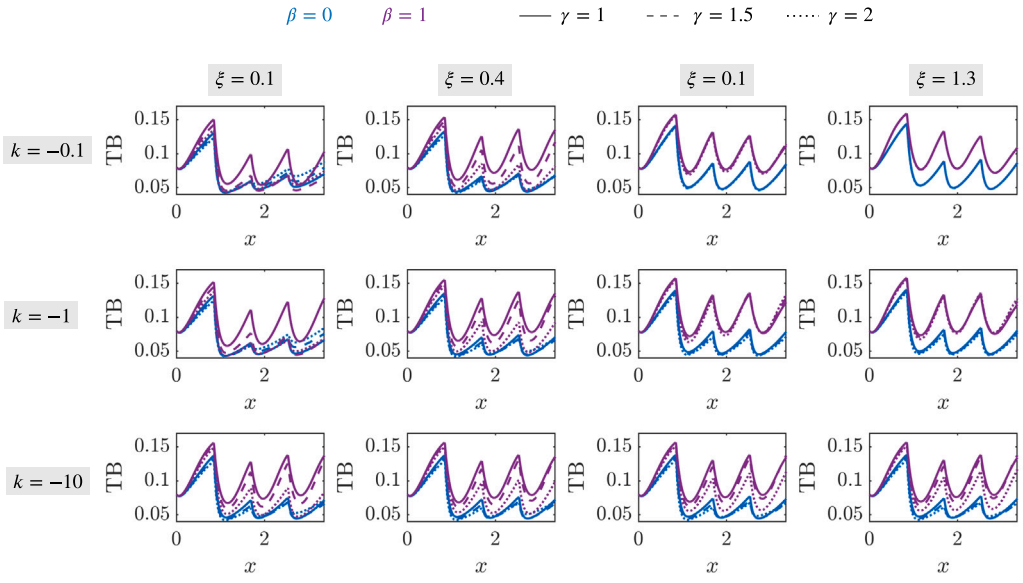

(a) Evolution of the TB.

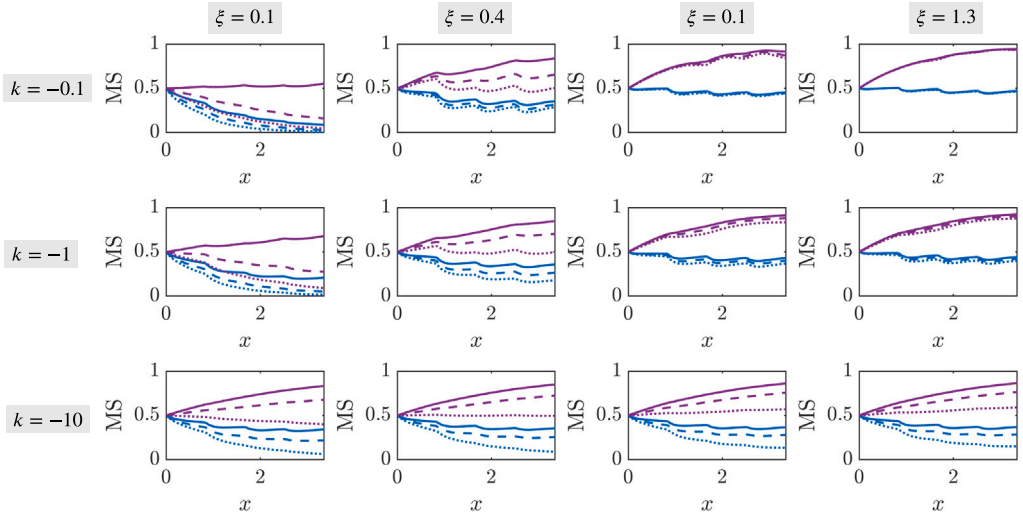

(b) Evolution of the MS.

Fig. 15. Evolution of TB and MS for an initial phenotypic state $v_0 = 0.5$. The grid shows simulations with different parameters related to the evolution of the phenotypic state. In particular, the location parameter in function ω increases from left to right, and the shape parameter k increases from bottom to top. In each subfigure, simulations for two different β values are plotted with different colours ($\beta = 0$ in blue and $\beta = 1$ in purple) and different values of the repair parameter γ are plotted with different line styles ($\gamma = 1$ with a continuous line, $\gamma = 1.5$ with a discontinuous line and $\gamma = 2$ with a dotted line).

Fig. 17 with the corresponding colour (blue for TB growth, yellow for TB regression and orange for tumour extinction), together with the simulation in constant hypoxia ($s_L(t) = s_R(t) = 0.14$) and constant normoxia ($s_L(t) = s_R(t) = 1.3$).

Interestingly, it can be seen that, although tumours composed of cells insensitive to phenotypic variations are generally bigger at the end of the simulation, they have a higher percentage of extinction. This suggests that phenotypic plasticity endows the tumours with a kind of resilience, even if that means being smaller in general, at least in what regards the number of alive cells.

Appendix C. Supplementary data

Supplementary material related to this article can be found online at https://doi.org/10.1016/j.compbiomed.2023.107291.

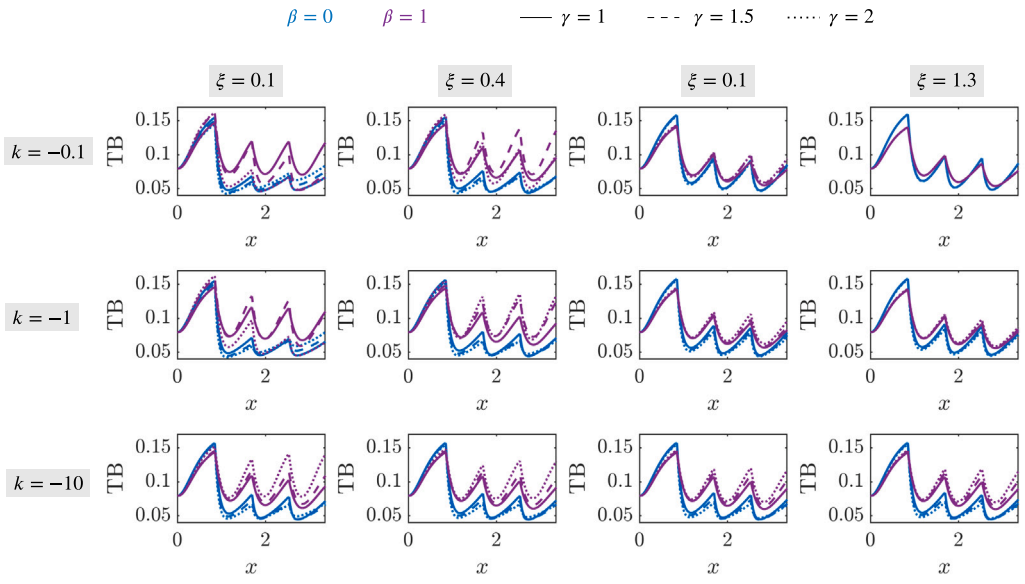

(a) Evolution of the TB.

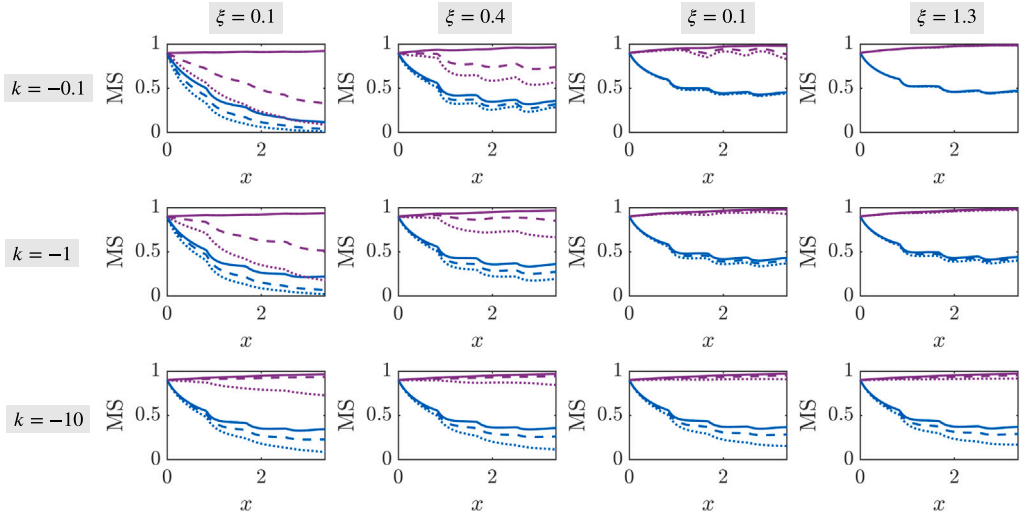

(b) Evolution of the MS.

Fig. 16. Evolution of TB and MS for an initial phenotypic state $v_0 = 0.9$. The grid shows simulations with different parameters related to the evolution of the phenotypic state. In particular, the location parameter in function ω increases from left to right, and the shape parameter k increases from bottom to top. In each subfigure, simulations for two different β values are plotted with different colours ($\beta = 0$ in blue and $\beta = 1$ in purple) and different values of the repair parameter γ are plotted with different line styles ($\gamma = 1$ with a continuous line, $\gamma = 1.5$ with a discontinuous line and $\gamma = 2$ with a dotted line).

Table 4
Summary of parameters and TB trends.

Case	$s_{\min}$	A	ϕ	TB (Scenario I)	TB (Scenario II)
1	Low (0.14)	Low (0.57)	Phase opposition (π)	Regression	Regression
2	Low (0.14)	Low (0.57)	$\pi/2$	Extinction	Regression
3	Low (0.14)	Low (0.57)	In phase (0)	Extinction	Extinction
4	Low (0.14)	High (1.14)	Phase opposition (π)	Growth	Growth
5	Low (0.14)	High (1.14)	$\pi/2$	Regression	Growth
6	Low (0.14)	High (1.14)	In phase (0)	Extinction	Regression
7	High (0.57)	Low (0.57)	Phase opposition (π)	Growth	Growth
8	High (0.57)	Low (0.57)	$\pi/2$	Growth	Growth
9	High (0.57)	Low (0.57)	In phase (0)	Growth	Growth
10	High (0.57)	High (1.14)	Phase opposition (π)	Growth	Growth
11	High (0.57)	High (1.14)	$\pi/2$	Growth	Growth
12	High (0.57)	High (1.14)	In phase (0)	Growth	Growth

Twelve representative configurations of the oxygen boundary conditions are considered, representing each possible trend.

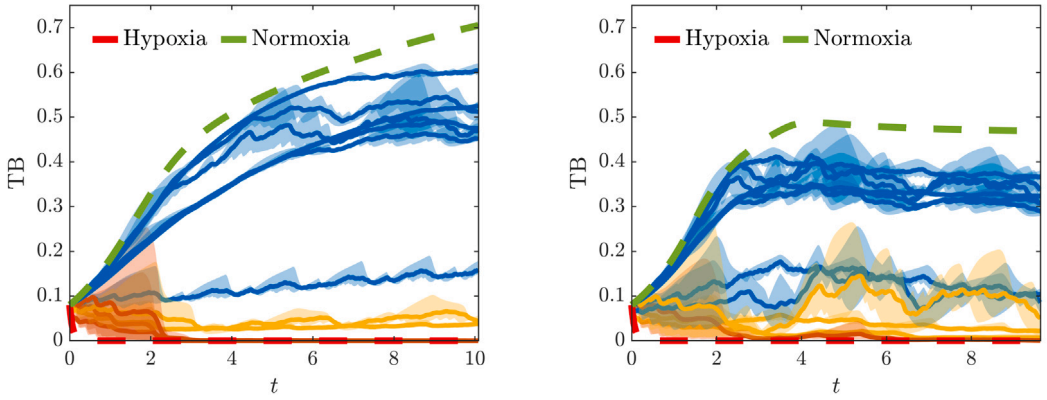

(a) Scenario I: Phenotype insensitive to oxygen variations.

(b) Scenario II: Phenotype sensitive to oxygen variations.

Fig. 17. TB evolution for the 12 cases detailed in Table 4. A blue line indicates that the TB at the end of the simulation is bigger than at the beginning, a yellow line indicates that it is smaller, and an orange line indicates that the tumour extincts. TB evolution in both constant hypoxia ($s_L(t) = s_R(t) = 0.14$) and constant normoxia ($s_L(t) = s_R(t) = 1.3$) are depicted in red and green respectively.

References

[1] R.J. Fox, J.M. Donelson, C. Schunter, T. Ravasi, J.D. Gaitán-Espitia, Beyond buying time: the role of plasticity in phenotypic adaptation to rapid environmental change, Phil. Trans. R. Soc. B 374 (1768) (2019) 20180174.

[2] H.F. Nijhout, Development and evolution of adaptive polyphenisms, Evol. Dev. 5 (1) (2003) 9–18.

[3] B. Xue, S. Leibler, Benefits of phenotypic plasticity for population growth in varying environments, Proc. Natl. Acad. Sci. 115 (50) (2018) 12745–12750.

[4] B.D. MacArthur, A. Ma'ayan, I.R. Lemischka, Systems biology of stem cell fate and cellular reprogramming, Nature Rev. Mol. Cell Biol. 10 (10) (2009) 672–681.

[5] X. Xu, Q. Wang, Y. Long, R. Zhang, X. Wei, M. Xing, H. Gu, X. Xie, Stress-mediated p38 activation promotes somatic cell reprogramming, Cell Res. 23 (1) (2013) 131–141.

[6] V. Olivier, N. Faucheux, P. Hardouin, Biomaterial challenges and approaches to stem cell use in bone reconstructive surgery, Drug Discov. Today 9 (18) (2004) 803–811.

[7] B.L. Beckstead, D.M. Santosa, C.M. Giachelli, Mimicking cell–cell interactions at the biomaterial–cell interface for control of stem cell differentiation, J. Biomed. Mater. Res. A Off. J. Soc. Biomater. Jpn. Soc. Biomater. Aust. Soc. Biomater. Korean Soc. Biomater. 79 (1) (2006) 94–103.

[8] M.M. Farag, Recent trends on biomaterials for tissue regeneration applications, J. Mater. Sci. 58 (2) (2023) 527–558.

[9] J. Kim, M. Samaranayake, S. Pradhan, Epigenetic mechanisms in mammals, Cell. Mol. Life Sci. 66 (2009) 596–612.

[10] E.J. Duncan, P.D. Gluckman, P.K. Dearden, Epigenetics, plasticity, and evolution: How do we link epigenetic change to phenotype? J. Exp. Zool. B Mol. Dev. Evol. 322 (4) (2014) 208–220.

[11] S. Shah, M. Rashid, T. Verma, S. Gupta, Chromatin, histones, and histone modifications in health and disease, Genome Plast. Health Dis. (2020) 109–135.

[12] F. Mohn, D. Schübeler, Genetics and epigenetics: stability and plasticity during cellular differentiation, Trends Genet. 25 (3) (2009) 129–136.

[13] R.R. Kanherkar, N. Bhatia-Dey, A.B. Csoka, Epigenetics across the human lifespan, Front. Cell Dev. Biol. 2 (2014) 49.

[14] A.P. Feinberg, Phenotypic plasticity and the epigenetics of human disease, Nature 447 (7143) (2007) 433–440.

[15] L. Chen, W. Huang, L. Wang, Z. Zhang, F. Zhang, S. Zheng, D. Kong, The effects of epigenetic modification on the occurrence and progression of liver diseases and the involved mechanism, Expert Rev. Gastroenterol. Hepatol. 14 (4) (2020) 259–270.

[16] P.A. Jones, S.B. Baylin, The fundamental role of epigenetic events in cancer, Nature Rev. Genet. 3 (6) (2002) 415–428.

[17] S.B. Baylin, P.A. Jones, A decade of exploring the cancer epigenome—biological and translational implications, Nat. Rev. Cancer 11 (10) (2011) 726–734.

[18] A. Biswas, S. De, Drivers of dynamic intratumor heterogeneity and phenotypic plasticity, Am. J. Physiol. Cell Physiol. 320 (5) (2021) C750–C760.

[19] D. Hanahan, Hallmarks of cancer: new dimensions, Cancer Discov. 12 (1) (2022) 31–46.

[20] P.B. Gupta, I. Pastushenko, A. Skibinski, C. Blanpain, C. Kuperwasser, Phenotypic plasticity: driver of cancer initiation, progression, and therapy resistance, Cell Stem Cell 24 (1) (2019) 65–78.

[21] T. Brabletz, R. Kalluri, M.A. Nieto, R.A. Weinberg, EMT in cancer, Nat. Rev. Cancer 18 (2) (2018) 128–134.

[22] S. Bhatia, P. Wang, A. Toh, E.W. Thompson, New insights into the role of phenotypic plasticity and EMT in driving cancer progression, Front. Mol. Biosci. 7 (2020) 71.

[23] H. Clevers, The cancer stem cell: premises, promises and challenges, Nat. Med. 17 (3) (2011) 313–319.

[24] L. Walcher, A.K. Kistenmacher, H. Suo, R. Kitte, S. Dluczek, A. Strauß, A.-R. Blaudszun, T. Yevsa, S. Fricke, U. Kossatz-Boehlert, Cancer stem cells—origins and biomarkers: perspectives for targeted personalized therapies, Front. Immunol. 11 (2020) 1280.

[25] J.N. Rich, Cancer stem cells: understanding tumor hierarchy and heterogeneity, Medicine 95 (Suppl 1) (2016).

[26] C. Scheel, R.A. Weinberg, Phenotypic plasticity and epithelial-mesenchymal transitions in cancer and normal stem cells? Int. J. Cancer 129 (10) (2011) 2310–2314.

[27] A.Z. Ayob, T.S. Ramasamy, Cancer stem cells as key drivers of tumour progression, J. Biomed. Sci. 25 (2018) 1–18.

[28] R.P. Hill, D.T. Marie-Egyptienne, D.W. Hedley, Cancer stem cells, hypoxia and metastasis, in: Seminars in Radiation Oncology, Vol. 19, No. 2, Elsevier, 2009, pp. 106–111.

[29] H. Axelson, E. Fredlund, M. Ovenberger, G. Landberg, S. Påhlman, Hypoxia-induced dedifferentiation of tumor cells–a mechanism behind heterogeneity and aggressiveness of solid tumors, in: Seminars in Cell & Developmental Biology, Vol. 16, No. 4–5, Elsevier, 2005, pp. 554–563.

[30] J. Heddleston, Z. Li, J.a. Lathia, S. Bao, A. Hjelmeland, J. Rich, Hypoxia inducible factors in cancer stem cells, Br. J. Cancer 102 (5) (2010) 789–795.

[31] T. Stanković, T. Ranđelović, M. Dragoj, S.S. Burić, L. Fernández, I. Ochoa, V.M. Pérez-García, M. Pešić, In vitro biomimetic models for glioblastoma-a promising tool for drug response studies, Drug Resist. Updates 55 (2021) 100753.

[32] A.R. Monteiro, R. Hill, G.J. Pilkington, P.A. Madureira, The role of hypoxia in glioblastoma invasion, Cells 6 (4) (2017) 45.

[33] D. Bergman, T.L. Jackson, Phenotype switching in a global method for agent-based models of biological tissue, PLoS One 18 (2) (2023) e0281672.

[34] V. Quaranta, K.A. Rejniak, P. Gerlee, A.R. Anderson, Invasion emerges from cancer cell adaptation to competitive microenvironments: quantitative predictions from multiscale mathematical models, in: Seminars in Cancer Biology, Vol. 18, No. 5, Elsevier, 2008, pp. 338–348.

[35] R.A. Gatenby, K. Smallbone, P.K. Maini, F. Rose, J. Averill, R.B. Nagle, L. Worrall, R.J. Gillies, Cellular adaptations to hypoxia and acidosis during somatic evolution of breast cancer, Br. J. Cancer 97 (5) (2007) 646–653.

[36] A. Ardaševa, R.A. Gatenby, A.R. Anderson, H.M. Byrne, P.K. Maini, T. Lorenzi, A mathematical dissection of the adaptation of cell populations to fluctuating oxygen levels, Bull. Math. Biol. 82 (2020) 1–24.

[37] A. Hodgkinson, L. Le Cam, D. Trucu, O. Radulescu, Spatio-Genetic and phenotypic modelling elucidates resistance and re-sensitisation to treatment in heterogeneous melanoma, J. Theoret. Biol. 466 (2019) 84–105.

[38] J.M. Ayuso, R. Monge, A. Martínez-González, M. Virumbrales-Muñoz, G.A. Llamazares, J. Berganzo, A. Hernández-Laín, J. Santolaria, M. Doblaré, C. Hubert, et al., Glioblastoma on a microfluidic chip: Generating pseudopalisades and enhancing aggressiveness through blood vessel obstruction events, Neuro-oncology 19 (4) (2017) 503–513.

[39] G.L. Celora, H.M. Byrne, P. Kevrekidis, Spatio-temporal modelling of phenotypic heterogeneity in tumour tissues and its impact on radiotherapy treatment, J. Theoret. Biol. 556 (2023) 111248.

[40] S.S. Hori, L. Tong, S. Swaminathan, M. Liebersbach, J. Wang, S.S. Gambhir, D.W. Felsher, A mathematical model of tumor regression and recurrence after therapeutic oncogene inactivation, Sci. Rep. 11 (1) (2021) 1–14.

[41] E. Ollier, P. Mazzocco, D. Ricard, G. Kaloshi, A. Idbaih, A. Alentorn, D. Psimaras, J. Honnorat, J.Y. Delattre, E. Grenier, et al., Analysis of temozolomide resistance in low-grade gliomas using a mechanistic mathematical model, Fundam. Clin. Pharmacol. 31 (3) (2017) 347–358.
[42] J.M. Greene, J.L. Gevertz, E.D. Sontag, Mathematical approach to differentiate spontaneous and induced evolution to drug resistance during cancer treatment, JCO Clin. Cancer Inform. 3 (2019) 1–20.
[43] J. Ayensa-Jiménez, M.H. Doweidar, T. Randelovic, L.J. Fernández, S. Oliván, I. Ochoa, M. Doblaré, On the simulation of organ-on-chip cell processes: Application to an in vitro model of Glioblastoma evolution, in: Advances in Biomechanics and Tissue Regeneration, Elsevier, 2019, pp. 313–341.
[44] J. Ayensa Jiménez, Study of the effect of the tumour microenvironment on cell response using a combined simulation and machine learning approach. Application to the evolution of Glioblastoma (PhD thesis), University of Zaragoza, 2022.
[45] S.A. Morris, The evolving concept of cell identity in the single cell era, Development 146 (12) (2019) dev169748.
[46] W.L. Brogan, Modern Control Theory, Pearson education india, 1991.
[47] M.F. Horstemeyer, D.J. Bammann, Historical review of internal state variable theory for inelasticity, Int. J. Plast. 26 (9) (2010) 1310–1334.
[48] M. Guo, Y. Peng, A. Gao, C. Du, J.G. Herman, Epigenetic heterogeneity in cancer, Biomark. Res. 7 (1) (2019) 1–19.
[49] J. Wright, Epigenetics: reversible tags, Nature 498 (7455) (2013) S10–S11.
[50] V. Blomen, J. Boonstra, Stable transmission of reversible modifications: maintenance of epigenetic information through the cell cycle, Cell. Mol. Life Sci. 68 (1) (2011) 27–44.
[51] H. Wu, Y. Zhang, Reversing DNA methylation: mechanisms, genomics, and biological functions, Cell 156 (1–2) (2014) 45–68.
[52] I. Lacal, R. Ventura, Epigenetic inheritance: concepts, mechanisms and perspectives, Front. Mol. Neurosci. 11 (2018) 292.
[53] K.A. Triantaphyllopoulos, I. Ikonomopoulos, A.J. Bannister, Epigenetics and inheritance of phenotype variation in livestock, Epigr. Chromatin 9 (1) (2016) 1–18.
[54] D. Stajic, L.E. Jansen, Empirical evidence for epigenetic inheritance driving evolutionary adaptation, Phil. Trans. R. Soc. B 376 (1826) (2021) 20200121.
[55] J. Ayensa-Jiménez, M. Pérez-Aliacar, T. Randelovic, S. Oliván, L. Fernández, J.A. Sanz-Herrera, I. Ochoa, M.H. Doweidar, M. Doblaré, Mathematical formulation and parametric analysis of in vitro cell models in microfluidic devices: application to different stages of glioblastoma evolution, Sci. Rep. 10 (1) (2020) 1–21.
[56] H. Hatzikirou, D. Basanta, M. Simon, K. Schaller, A. Deutsch, 'Go or grow': the key to the emergence of invasion in tumour progression? Math. Med. Biol. 29 (1) (2012) 49–65.
[57] B. Stramer, R. Mayor, Mechanisms and in vivo functions of contact inhibition of locomotion, Nature Rev. Mol. Cell Biol. 18 (1) (2017) 43–55.
[58] A.A. Patel, E.T. Gawlinski, S.K. Lemieux, R.A. Gatenby, A cellular automaton model of early tumor growth and invasion: the effects of native tissue vascularity and increased anaerobic tumor metabolism, J. Theoret. Biol. 213 (3) (2001) 315–331.
[59] J.M. Heddleston, Z. Li, R.E. McLendon, A.B. Hjelmeland, J.N. Rich, The hypoxic microenvironment maintains glioblastoma stem cells and promotes reprogramming towards a cancer stem cell phenotype, Cell Cycle 8 (20) (2009) 3274–3284.
[60] E. Batlle, H. Clevers, Cancer stem cells revisited, Nat. Med. 23 (10) (2017) 1124–1134.
[61] E.E. Bar, Glioblastoma, cancer stem cells and hypoxia, Brain Pathol. 21 (2) (2011) 119–129.
[62] L. Persano, E. Rampazzo, G. Basso, G. Viola, Glioblastoma cancer stem cells: role of the microenvironment and therapeutic targeting, Biochem. Pharmacol. 85 (5) (2013) 612–622.
[63] J.D. Lathia, S.C. Mack, E.E. Mulkearns-Hubert, C.L. Valentim, J.N. Rich, Cancer stem cells in glioblastoma, Genes Dev. 29 (12) (2015) 1203–1217.
[64] B. Ortensi, M. Setti, D. Osti, G. Pelicci, Cancer stem cell contribution to glioblastoma invasiveness, Stem Cell Res. Ther. 4 (1) (2013) 1–11.
[65] G. Iannolo, C. Conticello, L. Memeo, R. De Maria, Apoptosis in normal and cancer stem cells, Crit. Rev. Oncol. Hematol. 66 (1) (2008) 42–51.
[66] A. Filatova, T. Acker, B.K. Garvalov, The cancer stem cell niche (s): the crosstalk between glioma stem cells and their microenvironment, Biochim. Biophys. Acta BBA-Gen. Subj. 1830 (2) (2013) 2496–2508.
[67] E. Vlashi, C. Lagadec, L. Vergnes, T. Matsutani, K. Masui, M. Poulou, R. Popescu, L. Della Donna, P. Evers, C. Dekmezian, et al., Metabolic state of glioma stem cells and nontumorigenic cells, Proc. Natl. Acad. Sci. 108 (38) (2011) 16062–16067.
[68] R.D. Skeel, M. Berzins, A method for the spatial discretization of parabolic equations in one space variable, SIAM J. Sci. Stat. Comput. 11 (1) (1990) 1–32.
[69] M. Hofmann, Support vector machines-kernels and the kernel trick, Notes 26 (3) (2006) 1–16.
[70] W.R. Becker, S.A. Nevins, D.C. Chen, R. Chiu, A.M. Horning, T.K. Guha, R. Laquindanum, M. Mills, H. Chaib, U. Ladabaum, et al., Single-cell analyses define a continuum of cell state and composition changes in the malignant transformation of polyps to colorectal cancer, Nature Genet. 54 (7) (2022) 985–995.
[71] S.M. Groves, A.S. Ireland, Q. Liu, A.J. Simmons, K.S. Lau, W.T. Iams, D.R. Tyson, C.M. Lovly, T.G. Oliver, V. Quaranta, Cancer hallmarks define a continuum of plastic cell states between small cell lung cancer archetypes, bioRxiv (2021) https://api.semanticscholar.org/CorpusID:231777500.
[72] J. Lei, S.A. Levin, Q. Nie, Mathematical model of adult stem cell regeneration with cross-talk between genetic and epigenetic regulation, Proc. Natl. Acad. Sci. 111 (10) (2014) E880–E887.
[73] S. Murakami, Continuum Damage Mechanics: a Continuum Mechanics Approach to the Analysis of Damage and Fracture, Vol. 185, Springer Science & Business Media, 2012.
[74] G.A. Maugin, The saga of internal variables of state in continuum thermo-mechanics (1893–2013), Mech. Res. Commun. 69 (2015) 79–86.
[75] J.M. Ayuso, M. Virumbrales-Muñoz, A. Lacueva, P.M. Lanuza, E. Checa-Chavarria, P. Botella, E. Fernández, M. Doblare, S.J. Allison, R.M. Phillips, et al., Development and characterization of a microfluidic model of the tumour microenvironment, Sci. Rep. 6 (1) (2016) 1–16.
[76] Y. Hou, H. Guo, C. Cao, X. Li, B. Hu, P. Zhu, X. Wu, L. Wen, F. Tang, Y. Huang, et al., Single-cell triple omics sequencing reveals genetic, epigenetic, and transcriptomic heterogeneity in hepatocellular carcinomas, Cell Res. 26 (3) (2016) 304–319.
[77] B. Kakaradov, J. Arsenio, C.E. Widjaja, Z. He, S. Aigner, P.J. Metz, B. Yu, E.J. Wehrens, J. Lopez, S.H. Kim, et al., Early transcriptional and epigenetic regulation of CD8+ T cell differentiation revealed by single-cell RNA sequencing, Nature Immunol. 18 (4) (2017) 422–432.
[78] M. Shackleton, E. Quintana, E.R. Fearon, S.J. Morrison, Heterogeneity in cancer: cancer stem cells versus clonal evolution, Cell 138 (5) (2009) 822–829.
[79] M. Janiszewska, M.L. Suvà, N. Riggi, R.H. Houtkooper, J. Auwerx, V. Clément-Schatlo, I. Radovanovic, E. Rheinbay, P. Provero, I. Stamenkovic, Imp2 controls oxidative phosphorylation and is crucial for preserving glioblastoma cancer stem cells, Genes Dev. 26 (17) (2012) 1926–1944.
[80] C. Michiels, C. Tellier, O. Feron, Cycling hypoxia: A key feature of the tumor microenvironment, Biochim. Biophys. Acta (BBA)-Rev. Cancer 1866 (1) (2016) 76–86.
[81] C.H. Hsieh, W.C. Shyu, C.Y. Chiang, J.W. Kuo, W.C. Shen, R.S. Liu, NADPH oxidase subunit 4-mediated reactive oxygen species contribute to cycling hypoxia-promoted tumor progression in glioblastoma multiforme, PLoS One 6 (9) (2011) e23945.
[82] C.W. Chou, C.C. Wang, C.P. Wu, Y.J. Lin, Y.C. Lee, Y.W. Cheng, C.H. Hsieh, Tumor cycling hypoxia induces chemoresistance in glioblastoma multiforme by upregulating the expression and function of ABCB1, Neuro-oncology 14 (10) (2012) 1227–1238.